Connectivity reflects Coding: A Model of Voltage-based Spike-Timing-Dependent-Plasticity with Homeostasis

Claudia Clopath, Lars Büsing*, Eleni Vasilaki, Wulfram Gerstner

Laboratory of Computational Neuroscience
Brain-Mind Institute and School of Computer and Communication Sciences
Ecole Polytechnique Fédérale de Lausanne
1015 Lausanne EPFL, Switzerland
* permanent address: Institut für Grundlagen der Informationsverarbeitung, TU Graz, Austria

Abstract

Electrophysiological connectivity patterns in cortex often show a few strong connections, sometimes bidirectional, in a sea of weak connections. In order to explain these connectivity patterns, we use a model of Spike-Timing-Dependent Plasticity where synaptic changes depend on presynaptic spike arrival and the postsynaptic membrane potential, filtered with two different time constants. The model describes several nonlinear effects in STDP experiments, as well as the voltage dependence of plasticity. We show that in a simulated recurrent network of spiking neurons our plasticity rule leads not only to development of localized receptive fields, but also to connectivity patterns that reflect the neural code: for temporal coding paradigms with spatio-temporal input correlations, strong connections are predominantly unidirectional, whereas they are bidirectional under rate coded input with spatial correlations only. Thus variable connectivity patterns in the brain could reflect different coding principles across brain areas; moreover simulations suggest that plasticity is surprisingly fast.

Keywords: Synaptic plasticity, STDP, LTP, LTD, Voltage, Spike

Introduction

Experience-dependent changes in receptive fields[1-2] or in learned behavior relate to changes in synaptic strength. Electrophysiological measurements of functional connectivity patterns in slices of neural tissue[3-4] or anatomical connectivity measures[5] can only present a snapshot of the momentary connectivity -- which may change over time[6]. The question then arises whether the connectivity patterns and their changes can be connected to basic forms of synaptic plasticity[7] such as Long-Term Potentiation (LTP) and Depression (LTD) [8]. LTP and LTD depend on the exact timing of pre- and postsynaptic action potentials[9-10], but also on postsynaptic voltage[11-12], and presynaptic stimulation frequency[13]. Spike-Timing-Dependent Plasticity (STDP) has attracted particular interest in recent years, since temporal coding schemes where information is contained in the exact timing of spikes rather than mean frequency could be learned by a neural system using STDP[14-15] (review in[16]). However, the question whether STDP is more fundamental than frequency dependent plasticity or voltage dependent plasticity

rules has not been resolved, despite an intense debate[17]. Moreover it is unclear how the interplay of coding and plasticity yield the functional connectivity patterns seen in experiments. In particular, the presence or absence of bidirectional connectivity between cortical pyramidal neurons seems to be contradictory across experimental preparations in visual [3] or somatosensory cortex[4]. Recent experiments have shown that STDP is strongly influenced by postsynaptic voltage before action potential firing[18], but could not answer the question whether spike timing dependence is a direct consequence of voltage dependence, or the manifestation of an independent process. In addition, STDP depends on stimulation frequency[18] suggesting an interaction between timing and frequency dependent processes[18]. We show that a simple Hebbian plasticity rule that pairs presynaptic spike arrival with the postsynaptic membrane potential is sufficient to explain STDP and the dependence of plasticity upon presynaptic stimulation frequency. Moreover, the intricate interplay of voltage and spike-timing as well as the frequency dependence of STDP can be explained in our model from one single principle. In contrast to earlier attempts towards a unified description of synaptic plasticity[19-20], our model is a phenomenological one. It does not give an explicit interpretation in terms of biophysical quantities such a Calcium concentration[19], CaMKII[20], glutamate binding, NMDA receptors etc. Rather it aims at a minimal description of the major phenomena observed in electrophysiology experiments. The advantage of such a minimal model is that it allows us to discuss functional consequences in small[21-23], and possibly even large[24-25] networks. We show that in small networks of up to 10 neurons the learning rule leads to input specificity, necessary for receptive field development -- similar to earlier models of STDP[14,21] or rate-based plasticity rules[26-27]. Going significantly beyond earlier studies, we explicitly address the question of whether functional connectivity patterns of cortical pyramidal neurons measured in recent electrophysiological studies[3-4] could be the result of plasticity during continued stimulation of neuronal model networks, in particular bidirectional connections[3] which are incompatible with standard STDP models[21,23]. The mathematical simplicity of our model enables us to identify conditions under which it becomes equivalent to the well-known Bienenstock-Cooper-Munro (BCM) model[26] used in classical rate-based descriptions of developmental learning; and similar to some earlier models of STDP[28-29] -- and why our model is fundamentally different from classical STDP models[14,16,21], widely used for temporal coding.

1. Results

In order to study how connectivity patterns in cortex can emerge from plasticity, we need a plasticity rule that is consistent with a large body of experiments. Since synaptic depression and potentiation take place through different pathways[30] our model uses separate additive contributions to the plasticity rule, one for LTD and another one for LTP (see Fig. 1 and Methods).

1.1. Fitting the Plasticity Model to Experimental Data

Consistent with voltage clamp[12] and stationary depolarization experiment[11], LTD is triggered in our model if presynaptic spike arrival occurs while the membrane potential of the postsynaptic neuron is slightly depolarized (above a threshold θ_- usually set to resting potential) whereas LTP occurs if depolarization is big (above a second threshold θ_+, see Fig. 1). The mathematical formulation of the plasticity rule makes a distinction between the momentary voltage *u* and the low-pass filtered voltage variables $\bar{u}_-$ or $\bar{u}_+$ which denote temporal averages of the voltage over the recent past (the symbols $\bar{u}_-$

and $\bar{u}_+$ indicate filtering of *u* with two different time constants). Similarly, the event *x* of presynaptic spike arrival needs to be distinguished from the trace $\bar{x}$ that is left at the synapse after stimulation by neurotransmitter. Potentiation occurs only if the *momentary* voltage is above θ_+ (this condition is fulfilled during action potential firing) AND the *average* voltage $\bar{u}_+$ above θ_- (this is fulfilled if there was a depolarization in the recent past) AND the trace $\bar{x}$ left by a previous presynaptic spike event is nonzero (this condition holds if a presynaptic spike arrived a few milliseconds earlier at the synapse; Fig. 1b). LTD occurs if the average voltage $\bar{u}_-$ is above θ_- at the moment of a presynaptic spike arrival (see Fig. 1a). The amount of LTD in our model depends on a homeostatic process on a slower time scale [31]. Low-pass filtering of the voltage by the variable ($\bar{u}_-$ or $\bar{u}_+$) refers to some unidentified intracellular processes triggered by depolarization, e.g., increase in calcium concentration or second messenger chains. Similarly, the biophysical nature of the trace $\bar{x}$ is irrelevant for the functionality of the model, but a good candidate process is the fraction of glutamate bound to postsynaptic receptors.

We simulated a STDP protocol, where presynaptic spikes arrive a few milliseconds before or after a postsynaptic spike. If a post-pre pairing with a timing difference of 10 milliseconds is repeated at frequencies below 35Hz, LTD occurs in our model (Fig. 2a, b), consistent with experiments [18]. Repeated pre-post pairings (with 10 millisecond timing difference) at frequencies above 10Hz yield LTP, but pairings at 0.1Hz do not show any significant change in the model or in experiments [18]. In the model these results can be explained by the fact that at 0.1Hz repetition frequency, the low-pass filtered voltage $\bar{u}_+$ which increases abruptly during postsynaptic spiking decays back to zero before the next impulse arrives, so that LTP cannot be triggered. However, since LTD in the model requires only a weak depolarization of $\bar{u}_-$ at the moment of presynaptic spike arrival, post-pre pairings give rise to depression, even at very low frequency. At repetition frequencies of 50Hz, the post-pre paradigm is nearly indistinguishable from a pre-post timing, and LTP dominates.

If a pre-post protocol at 0.1Hz, that normally does not induce LTP, is combined with a depolarizing current pulse, then potentiation is observed in experiments [18] and in our model (Fig. 2 c, f, i). Due to the injected current, the low-pass filtered voltage variable $\bar{u}_+$ is depolarized before the pairing. Thus at the moment of the postsynaptic spike, the average voltage $\bar{u}_+$ is above the threshold ϑ_-, leading to potentiation. Similarly, a pre-post protocol that normally leads to LTP can be blocked if the postsynaptic spikes are triggered on the background of a hyperpolarizing current (Fig. 2 e, h, i).

In order to study nonlinear aspects of STDP, we simulate a protocol of burst-timing-dependent plasticity where presynaptic spikes are paired with 1, 2 or 3 postsynaptic spikes[32] (see Methods). Whereas pairings at 0.1Hz do not change the synaptic weight, repeated triplets pre-post-post generate potentiation in our model because the first postsynaptic spike induces a depolarizing spike after potential so that $\bar{u}_+$ is depolarized. Adding a third postsynaptic spike to the protocol (i.e., quadruplets pre-post-post-post) does not lead to stronger LTP (Fig. 3a). Our model also describes the dependence of LTP upon the intra-burst frequency (Fig. 3b). At an intra-burst frequency of 20Hz, no LTP occurs, because the second spike in the burst comes so late that the presynaptic trace $\bar{x}$ has decayed back to zero. At higher intra-burst frequencies, the three conditions for LTP ($u(t)>\vartheta_+$ and $\bar{u}_+>\vartheta_-$ and $\bar{x}>0$) are fulfilled. The

burst timing dependence (Fig. 3c) where the timing of one presynaptic spike is changed with respect to a burst of three postsynaptic spikes is qualitatively similar to that found in experiments[32-33], but only four of the six experimental data points are quantitatively reproduced by the model with a given set of parameters. Interestingly, our model predicts that the curve of burst-timing dependent plasticity should show a significant change in the amount of potentiation whenever the presynaptic spike is shifted across one of the three postsynaptic spikes (Fig. 3c). Since dendritic spikes which are relevant for burst-timing dependent STDP[33] are broader than somatic action potentials, the 'jumps' in the burst-STDP curves would be blurred.

2.2 Functional implications

Connectivity patterns in a local cortical circuit have been shown to be non-random, i.e. the majority of connections are weak and the rare strong ones have a high probability of being bidirectional[3]. However, standard models of STDP [16] do not exhibit stable bidirectional connections[23,34]. Intuitively, if the cell A fires before the cell B, a pre-post pairing for the 'AB' connection is formed so that the connection is strengthened. The post-pre pairing occurring at the same time in the 'BA' connection leads to depression. Therefore it is impossible to strengthen both connections at the same time. Moreover, in order to assure long-term stability of firing rates, parameters in standard STDP rules are typically chosen such that inhibition slightly dominates excitation[16] which implies that random spike firing decreases connections. However, the nonlinear aspects of plasticity in our model change such a simple picture. From Fig. 2b and 3b we expect that at higher neuronal firing rates, our model could develop stable bidirectional connections, in contrast to standard STDP rules.

We first simulated a small network of 10 all-to-all connected neurons where each neuron fires at a fixed frequency, but the frequency varies across neurons. We find that bidirectional connections are formed only between those neurons that both fire at a high rate (Fig. 4a). In a second paradigm, the neurons in the same network are stimulated cyclically such that they are firing in a distinct temporal order (1, 2 , 3,..). In that case, the weights form, after a period of synaptic plasticity, a loop where strong connections from 1 to 2, 2 to 3 ... develop, but no bidirectional connections (Fig. 4b). These results are in contrast to simulation experiments with a standard STDP rule, where connections are always unidirectional, independently of the stimulation paradigm (Fig. 4c, d). Theoretical arguments (see Supplementary Methods) show that bidirectional connections cannot exist under the cyclic temporal stimulation paradigm (neither for standard STDP nor for our plasticity model). Bidirectional connections do develop in our nonlinear voltage dependent plasticity model under the assumption of slowly varying rates -- in contrast to standard STDP (Fig. 4c, d).

To move to a more realistic scenario, we simulated a network of 10 excitatory neurons (with all-to-all connectivity) and 3 inhibitory neurons. Each inhibitory neuron receives input from 8 randomly selected excitatory neurons and randomly projects back to 6 excitatory neurons. In addition to the recurrent input, each excitatory and inhibitory neuron receives feedforward spike input from 500 presynaptic neurons j that generate stochastic Poisson input at a rate ν_j. The rates of neighboring input neurons are correlated, mimicking the presence or absence of spatially extended objects. The location of the stimulus is switched every 100ms to a new random position. In case of retinal input, this would

correspond to a situation where the subject fixates every 100ms on a new stationary stimulus. Depending on the retinal position of stimulus, a given postsynaptic neuron responds with low, medium, or high firing rate which is stationary during the 100ms stimulation period; the firing rates of the 10 neurons in the network encode the current position of the stimulus (rate coding paradigm). In a temporal-coding paradigm, the model input is shifted every 20ms to a neighboring location, mimicking rapid movement of an object across an array of sensory receptors, e.g., during whisking behavior[35]. In this scenario, a given model neuron exhibits only short transient bursts of a few spikes so that it is the temporal structure of the activity (as opposed to stationary firing rates) that encode the position and movement of the stimulus. For both scenarios the network is identical. Feedforward connections and lateral connections between model pyramidal neurons are plastic whereas connections to and from inhibitory neurons are fixed.

During the first 100 - 400 seconds of stimulation with the rate-coding paradigm, the excitatory neurons develop localized receptive fields, i.e., weights from *neighboring* inputs to the same postsynaptic neuron become either strong or weak *together* and stay stable thereafter (Fig. 5a). Similarly, lateral connections onto the same postsynaptic neuron develop to strong or weak synapses, that remain, apart from fluctuations, stable thereafter (Fig. 5a) leading to a structured pattern of synaptic connections (Fig. 5b). After reordering the neurons according to similarity of receptive fields, we can clearly distinguish that three groups of neurons have been formed, characterized by strong bidirectional connectivity within the group, and different receptive fields and no lateral connectivity between groups (Fig. 5c). If the overall amplitude of plastic changes is small (compared to that found in the experiments), the pattern of lateral connectivity is stable and shows a few strong bidirectional connections in a sea of weak lateral connectivity. The reason is that two neurons with similar receptive fields are both active at high rate whenever the stimulus is in the center region of their receptive field which gives rise to strong bidirectional lateral connections (compare Fig. 4). Unidirectional strong connections are nearly absent (Fig. 5c and d). If the amplitude and rate of plasticity is more realistic and in agreement with the data of Fig. 2, then the pattern of lateral connectivity changes between one snapshot and another one 5 seconds later, but the overall pattern is stable when averaged over 100s (Fig. 5f-h). In each snapshot, about half of the strong connections are bidirectional (Fig. 5h and i).

This connectivity pattern contrasts with that shown under a temporal coding paradigm (Fig. 6). Neurons develop receptive fields similar to those seen with the rate-coding paradigm, but as expected for temporal Hebbian learning[16] the receptive field shifts over time (Fig. 6a). With small learning rate this shift is slow, as in previous models[16] but with realistic learning parameters extracted from the experiments in Fig. 2, the shift of the receptive field is surprisingly rapid (Fig. 6a, lower panel). More importantly, amongst the lateral connections, strong reciprocal links are nearly absent, whereas strong unidirectional connections from neuron n to neuron $n+1, n+2, n+3$ dominate (Fig. 6b-e). As the pattern of feedforward connections forming the receptive fields changes, the structure of lateral connections changes as well on the time scale of 10 minutes. Nevertheless, at each moment in time, the pattern of lateral connections is highly asymmetric, favoring connections from neuron n to $n+k$ (with $k=1,2,3$) over those from n to $n-k$, where n is the neuronal index after relabeling according the receptive field position (Fig. 6a). This suggests that temporal coding paradigms where stimuli are non-stationary and exhibit

systematic spatio-temporal correlations, are reflected in the functional connectivity pattern by strong uni-directional connections whereas rate coding (characterized by stationary input with spatial correlations only) leads to strong bidirectional connections. We have confirmed this for a broad range of stimuli and also in the presence of noise (Suppl. Figs. S1,S2).

2.3 Development of localized receptive fields and relation to rate models

The results for the feedforward connectivity in the previous subsection lead to the question of the behavior of our plasticity model under stimulation paradigms previously used for rate models [26,36-37]. Both our spiking rule and the rate-based BCM model[26] require presynaptic activity in order to induce a change. Furthermore, for our rule as well as for the simplest BCM rule (see[26]), the depression terms are linear and the potentiation terms are quadratic in the postsynaptic variables (i.e., the postsynaptic potential or the postsynaptic firing rate). More quantitatively, for Poisson input the total weight change Δw in our model is proportional to $v^{pre}\, v^{post}\, (v^{post} - \vartheta)$ where v^{pre} and v^{post} denote the firing rates of pre- and postsynaptic neurons, respectively, and ϑ is a sliding threshold related to the ratio between the LTP and LTD inducing processes (see Methods, Eq. 8). The sliding threshold arises in our plasticity model because the amount of LTD A_{LTD} depends on the long-term average of the voltage on the slow time scale of homeostatic processes. Due to its similarities to BCM, it is not surprising that our spike-based learning rule with sliding threshold is able to support the development of localized receptive fields, a feature related to independent component analysis (ICA) and sparse coding[26,36]. In our experiments, the input consists of small patches of natural images using standard preprocessing[37]. After learning with our plasticity rule, the weights exhibit a stable spatial structure that can be interpreted as a receptive field (Fig. 7). In contrast to a principal component analysis of image patches (as for example implemented by Hebbian learning in linear neurons[38]), the receptive fields are *localized* (i.e. the region with significant weights does not stretch across the whole image patch). Nine runs of the learning experiments give receptive fields with different locations and orientations (Fig. 7d). Because of the homeostatic control of LTD in our plasticity model, the neuron compensates in experiments with increased input firing rates by developing smaller receptive fields that are even more localized (Fig. 7e). Development of localized receptive fields has been interpreted as a signature of ICA or sparse coding[37]. In contrast to most other ICA algorithms[39] our rule is biologically more plausible since it is consistent with a large body of plasticity experiments.

2. Discussion

Because traditional plasticity rules are rate models, the relation between coding and connectivity could not be studied. Our plasticity rule is formulated on the level of postsynaptic voltage. Since action potentials are sharp voltage peaks, they act as singular events in the voltage so that, in the presence of a spike, our rule turns automatically into a spike-timing dependent rule. Indeed, for spike coding (and without subthreshold voltage manipulations) our plasticity rule behaves like a STDP rule where triplets of spikes with pre-post-post or post-pre-post timing evoke LTP[28-29], whereas pairs with post-pre timing evoke LTD. In contrast to standard STDP rules (reviewed in[16]), pairing frequency dependence[18] and burst-timing dependence[32] are qualitatively described. In addition the rule is expected to reproduce the

triplet and quadruplet experiments in hippocampal slices[40] (data not shown), because for all STDP protocols the plasticity rule in this paper is similar to an earlier nonlinear STDP rule[29]. Deriving STDP rules from voltage dependence has been attempted before[18,41-42]. However, since these earlier models use the momentary voltage[42] or its derivative[41], rather than a combination of momentary and averaged voltage as in our model, these earlier models cannot account for the broad range of nonlinear effects in STDP experiments or interaction of voltage and spike-timing. The voltage-based model of Sjöström[18] uses separate empirical functions for timing dependence, voltage dependence, frequency dependence, and multiple spike summation with preference for LTP, to capture the nonlinear effects of LTP. Our model is similar in that it also uses momentary voltage before the spike as one of the variables, but requires neither an explicit frequency-dependent, nor an explicit timing-dependent term. Rather, frequency and timing dependence follow from the model dynamics. Our model shows similarities with LTP induction in the TagTriC model[43], but the TagTriC model focuses on the long-term stability of synapses, rather than spike timing dependence of the induction mechanism.

Even though our model does not require a biophysical interpretation of the variables, it is tempting to speculate about potential mechanisms. For the *depression* term in our model, a 'trace' $\bar{u}_-$ left by previous activity of the postsynaptic neuron is combined with spike arrival *x* at the presynaptic terminal (Fig. 1a). In view of the results on LTD in layer-V neocortical neurons[44], this trace could be related to endocannabinoids released from the postsynaptic site. Coincidence of this slow trace with the activation of presynaptic NMDA receptors (which rapidly respond to the glutamate released by presynaptic activity *x(t)*) could be the trigger signal for LTD[44]. Indeed, the duration of the LTD part in the STDP function increases, if the endocannabinoid trace is artificially prolonged (see Fig 9 of[44]). In other neuron types and brain areas, the same mathematical model (but with different parameters) could correspond to different biophysical mechanisms of LTD. For example, in hippocampal CA1 neurons, the trace $\bar{u}_-$ could reflect the calcium entry through voltage-gated ion channels during depolarization which, when combined with synaptic signals (caused by the presynaptic spike arrival *x*), would give rise to calcium signals necessary to trigger LTD (reviewed in[19-20,44]). *Potentiation* is induced in our model by the combination of three factors: a momentary depolarization above spike threshold; a depolarization just before the spike, $\bar{u}_+$, above rest; and the presence of a 'trace' $\bar{x}$ left by presynaptic spike arrival (Fig. 1a). The trace $\bar{x}$ could correspond to the amount of glutamate bound to the postsynaptic NMDA receptor but this is controversial[44]. A high momentary voltage *u* can be induced by a backpropagating action potential; interestingly, backpropagation of action potentials is more likely and more reliable to occur in the background of a weak depolarization of the dendrite[44] -- and such a weak depolarization potentially corresponds to the term $\bar{u}_+$ in our model. Because in our model we have a depolarizing afterpotential after each spike (Fig. 1c, similar to that seen in experiments Fig. 1d), the value of $\bar{u}$ just before the next spike increases with the repetition frequency of the STDP protocol, in agreement with experiments (Fig. 5D in[44]). Our model is therefore consistent with results that LTP can be induced in distal synapses only if additional cooperative input or dendritic depolarization prevent failure of backpropagating action potentials[45]. In the context of the classical view of the NMDA receptor as a coincidence detector[44], it is quite natural to see why a sequence post-pre-post of two postsynaptic action potentials and one presynaptic spike are ideal for LTP: The spike-afterpotential of the first postsynaptic action potential

removes the calcium block and prepares the dendrite for successful backpropagation of a later action potential. If the backpropagating action potential caused by the second postsynaptic spike occurs just slightly after presynaptic spike arrival, this causes a sharply peaked and large calcium transient that would be sufficient to trigger the LTP induction chain.

Even though our model is formulated on the level of voltage, we do not imply that voltage itself is the essential biophysical mechanism. Rather, under physiological conditions, the voltage transient (or current or conductance transient) caused by synaptic input or action potential firing is the starting point of long biochemical signaling chains that, in the end lead to induction of plasticity. In our phenomenological model, the signature of the inputs (here: voltage transients) are directly linked (via mathematical variables or 'traces') to the induction of plasticity, jumping over the biophysical mechanisms of the signal transduction chain.

Our plasticity rule allows us to explain experiments from two different laboratories by one single principle. Both the ``potentiation is rescued by depolarization'' [18] scenario (Fig. 2f) and that of burst-timing dependent LTP[32] (Fig. 3) show that LTP at low frequency is induced when the membrane is depolarized before the pre-post pairing. This depolarization can be due to a previous spike during a postsynaptic burst[32] or to a depolarization current. A further unexpected result is that, with the set of parameters derived from visual cortex slice experiments, synapses fluctuate rapidly between strong and weak weights. This aspect is interesting in view of synapse mobility reported in imaging experiments[6].

Possible extensions of the model include a weight dependence of synaptic plasticity. We assumed that weights can grow to a hard upper bound, but the rule can easily be changed to soft bounds[16] by changing the prefactors A_{LTP}, A_{LTD} accordingly[43]. Second, short-term plasticity[46] could be added for a better description of the plasticity phenomena occurring especially during high frequency protocols. Third, additional mechanisms need to be implemented to describe the transition from early to late LTP/LTD [43,47]. Finally, we can generalize from point neurons to spatially extended neurons using a multi-compartment neuron model (e.g. distinct compartments for the soma and dendrites). In the presented work we did not do this, because detailed spatial models introduce a considerable number of new parameters making overfitting more likely to occur. Interestingly, our voltage-based formulation of plasticity, if applied locally in a compartmental model would allow potentiation to occur in a dendritic branch whenever the three conditions: presynaptic activity, recent postsynaptic depolarization, and momentary large depolarization occur together --- independent of the source of depolarization. Hence, dendritic spikes could lead to potentiation in the absence of somatic action potentials, in agreement with experiments in hippocampal[48-50] and cortical slices[33].

Our plasticity model leads to several predictions that could be tested in slice experiments. First, the model predicts that in voltage clamp experiments the weight change is only dependent on the voltage and the *number* of presynaptic spikes but not on their exact timing (e.g., low frequency, tetanus, or burst). Second, in the scenario where potentiation is rescued by depolarization, the amount of weight change should be the same whether a depolarizing current of amplitude B stops precisely when the postsynaptic spike is triggered or whether a current of slightly bigger amplitude B' stops a few milliseconds earlier.

The influence of STDP on temporal coding has been studied in the past primarily with respect to changes in the feedforward connections (reviewed in[16]). The effect of STDP on lateral connectivity has been studied much less[22-25]. We have shown in this paper that, because of STDP, coding influences the network topology, i.e. different stimulation paradigms generate different patterns of lateral connectivity. Our results are in contrast to standard STDP rules which always suppress short loops, and in particular bidirectional connections[23,34]. Our more realistic plasticity model shows that under a rate coding paradigm (where the neuron is stimulated by different stationary patterns) bidirectional connectivity and highly connected clusters with multiple loops are not only possible, but even dominant. It is only for temporal coding (characterized by stimulation with significant spatiotemporal correlations), that our biologically plausible rule leads to dominant unilateral directions. We speculate that the differences in coding between different brain areas could lead, even if the learning rule were exactly the same, to different network topologies. Our model predicts that experiments where cells in a recurrent network are repeatedly stimulated in a fixed order would decrease the fraction of strong bidirectional connections, whereas a stimulation pattern where clusters of neurons fire at high rate during episodes of a few hundred milliseconds would increase this fraction. In this view it is tempting to connect the low degree of bidirectional connectivity in barrel cortex[4] to the bigger importance of temporal structure in whisker input[35], compared to visual input.

3. Acknowledgments

Supported by the European projects FACETS and the Swiss National Science Foundation.

4. Figure Captions

Caption 1: Illustration of the model. Synaptic weights react to presynaptic events (top) and postsynaptic membrane potential (bottom). a. The synaptic weight is decreased if a presynaptic spike *x* (green) arrives when the low pass filtered value $\bar{u}_-$ (magenta) of the membrane potential is above θ_- (dashed horizontal line). b. The synaptic weight is increased if the membrane potential *u* (black) is above a threshold θ_+ and the low pass filtered value of the membrane potential $\bar{u}_+$ (blue) higher than a threshold θ_- as well as the presynaptic low pass filter $\bar{x}$ (orange) non zero. c. Step current injection makes the postsynaptic neuron fire at 50Hz in the absence of presynaptic stimulation (membrane potential *u* in black). No weight change is observed. Note the depolarizing spike-afterpotential consistent with experimental data d., reproduced from [18]. e-h. Voltage clamp experiment. A neuron receives weak presynaptic stimulation of 2Hz during 50s while the postsynaptic voltage is clamped to values between -60mV and 0mV. e-g. Schematic drawing of the trace $\bar{x}$ (orange) of the presynaptic spike train (green) as well as the voltage (black) and the synaptic weight (blue) for hyperpolarization (e), slight depolarization (f) and large depolarization (g). h. The weight change as a function of clamped voltage using the standard set of parameters for visual cortex data (dashed blue line, voltage paired with 25 spikes at the synapse). With a different set of parameters the model fits experimental data (red circles) in hippocampal slices [12], see Methods for details.

Caption 2: a-b. Simulated STDP experiments. a. Spike-timing dependent learning window: synaptic weight change for different time intervals *T* between pre- and postsynaptic firing using 60 pre-post-pairs at 20Hz. b. Weight change as a function of pairing repetition frequency ρ using pairings with a time delay of +10ms (pre-post, blue) and -10ms (post-pre, red). Dots represent data from Sjöström et al.[18] and lines the plasticity model. c-i. Interaction of voltage and STDP. c-e. Schematic induction protocols (green: presynaptic input, black: postsynaptic current, blue: evolution of synaptic weight). c. Low-Frequency Potentiation is rescued by depolarization[18]. Low frequency (0.1Hz) pre-post spike pairs yield LTP if a 100ms-long depolarized current is injected around the pairing. d. LTP fails if an additional brief hyperpolarized pulse is applied 14ms before postsynaptic firing so that voltage is brought to rest. e. Hyperpolarization preceding action potential prevents potentiation that normally occurs at 40Hz[18]. f. The simulated postsynaptic voltage *u* (black) following protocol c together with temporal averages $\bar{u}_-$ (magenta) and $\bar{u}_+$ (blue). Presynaptic spike time indicated by green arrow. Using the model (Eq. 3) this setting gives potentiation. g. Same as f, but following protocol d. No weight change is measured. h. Same as f., but following protocol e. No weight change is measured. i. Histogram summarizing the normalized synaptic weight of the simulation (bar) and the experimental data[18] (dot, blue bar=variance) for 0.1Hz pairing (control 1); 0.1Hz pairing with the depolarization (protocol c.); 0.1Hz pairing with the depolarization and brief hyperpolarization (protocol d.); 40Hz pairing (control 2); 40Hz pairing with the constant hyperpolarization (protocol e.); parameters in table 1b.

Caption 3: Burst-timing-dependent plasticity. One presynaptic spike is paired with a burst of postsynaptic spikes. This pairing is repeated 60 times at 0.1Hz. a. Normalized weight as a function of the number of postsynaptic spikes (1, 2, 3) at 50Hz. (dots: data from [32], crosses: simulation). The presynaptic spike is paired +10ms before the first postsynaptic spike (blue) or -10ms after (red). b. Normalized weight as a function of the frequency between the three postsynaptic action potentials (dot: data, lines: simulation; blue: pre-post, red: post-pre). c. Normalized weight as a function of the timing between the presynaptic spike and the first postsynaptic spike of a 3-spike burst at 50Hz (dot: data, black lines: simulation). A hard upper bound has been set to 250% normalized weight. The dashed line/crosses and the dotted line/stars represent simulations with alternative sets of parameters, respectively A_{LTD} =21e^{-5}mV^{-1}, A_{LTP} =50e^{-4}mV^{-2}, τ_x =143ms, τ_- =6ms, τ_+ =5ms and A_{LTD} =21e^{-5}mV^{-1}, A_{LTP} =67e^{-4}mV^{-2}, τ_x =5ms, τ_- =8ms, τ_+ =5ms. Shading: reachable data points generated by the model with different parameters.

Caption 4: Weight evolution in a all-to-all connected network of 10 neurons. a. Rate code: Neurons fire at different frequencies, neuron 1 at 2Hz, neuron 2 at 4Hz... neuron 10 at 20Hz. The weights (bottom) averaged over 100s show that neurons with high firing rates develop strong bidirectional connections (light blue: weak connections (under 2/3 of the maximal value); yellow: strong unidirectional connections (above 2/3 of the maximal value); brown: strong bidirectional connections). The cluster is schematically represented on top ("after"). b. Temporal code: Neurons fire successively every 20ms

(neuron 1 then 20ms later neuron 2, then 3...). Connections (bottom) are unidirectional with strong connections from presynaptic neuron with index n (vertical axis) to postsynaptic neuron with index n+1, n+2 and n+3 leading to a ring-like topology (top: schematic). c. d. Same but with standard STDP rule [14,16,21]. Bidirectional connections are impossible.

Caption 5: Plasticity during rate coding. a. A network of 10 excitatory (light blue) and 3 inhibitory neurons (red) receives feedforward inputs from 500 Poisson spike trains with a Gaussian profile of firing rates. The center of the Gaussian is shifted randomly every 100ms. (Schematical network before (left) and after the plasticity experiment (right)). The panels show the temporal evolution of the weights (upper panels: small amplitudes of plasticity, lower panels: normal amplitudes of plasticity, left panels: feedforward connections onto neuron 1; right panel: recurrent connections onto neuron 1). b-e. Learning with small amplitudes. Parameters as in Table 1b (visual cortex data) except for the amplitudes A_{LTP} and A_{LTD} which are reduced by a factor 100. b. Mean feedforward weights (left) and recurrent excitatory weights (right) averaged over 100s. Feedforward weights (left) indicate that neurons develop localized receptive fields (light grey). The recurrent weights (right) are classified into: light blue - weak (less than 2/3 of the maximal weight), yellow - strong (more than 2/3 of the maximal weight) unidirectional, brown - strong reciprocal connections. The diagonal is white, since self-connections do not exist in the model. c. Same as (b) but neuron index reordered. d. Three snap shots of the recurrent connections taken 5s apart indicate that recurrent connections are stable. e. Histogram of reciprocal, unidirectional and weak connections in the recurrent network averaged over 100s as in (b). The total number of weight fluctuations during 100s is zero (noted on the figure). The histogram shows an average of 10 repetitions (errorbars are the standard deviation). f-i. Rate code during learning with normal amplitudes. Same network as before but standard set of parameters (Table 1b, visual cortex). f. Receptive fields are localized; g. Reordering shows clusters of neurons with bidirectional coupling. These clusters are stable when averaged over 100 seconds, but h. connections can change from one time step to the next. i. The percentage of reciprocal connections is high, but because of fluctuations (fluc) more than 1000 transitions between strong unidirectional to strong bidirectional or back occur during 100 seconds.

Caption 6: Temporal coding paradigm. Same setting as in Fig. 5 (parameters from Table 1b, visual cortex) but input patterns are moved successively every 20ms, corresponding to a step-wise motion of the Gaussian stimulus profile across the input neurons. a. The schematic figure shows the network before and after the plasticity experiment. Panels show the temporal evolution of the weights (upper panel: amplitude of synaptic plasticity for feedforward connections reduced by a factor of 100; left feedforward weights onto neuron 6; right: lateral connections onto neuron 6. Lower panel: normal amplitude of plasticity, left panel: feedforward connections onto neuron 1 right panel: temporal evolution of asymmetry index of connection pattern (grey line: asymmetrical index for simulation Fig. 5). Positive values indicate the weights from neurons n to $n+k$ are stronger than those from n to $n-k$ for $1 \leq k \leq 3$). b. Receptive fields are localized (left). The recurrent network develops a ring-like structure with strong unidirectional connections from neuron 8 (vertical axis) to neuron 9 and 10 (horizontal axis) etc

(small amplitudes of plasticity). c: Same as b, but normal plasticity values. d. Some of the strong unilateral connections appear or disappear from one time step to the next, but the ring-like network structure persists, since the lines just above the diagonal are much more populated than the line below the diagonal. E. Reciprocal connections are absent, but unidirectional connections fluctuate several times between 'weak' and 'strong' during 100s.

Caption 7: a. A small patch of 16x16 pixels is chosen from the whitened natural images benchmark[37]. The patch is selected randomly and is presented as input to 512 neurons for 200ms. The positive part of the image is used as the firing rate to generate Poisson spike trains of the 256 "ON" inputs and the negative one for the 256 "OFF" inputs. b. The weights after convergence are shown for the "ON" inputs and the "OFF" inputs rearranged on a 16x16 image. The filter is calculated by subtracting the "OFF" weights from the "ON" weights. The filter is localized and bimodal, corresponding to an oriented receptive field. c. Temporal evolution of the weights shown in the red dashed box in panel b. d. Nine different neurons. e. Two different neurons receiving presynaptic input with varying firing rates from (top) 0-25Hz (middle) 0-37.5Hz (bottom) 0-75Hz.

Caption Table 1: a. Parameters for the neuron model. b. Plasticity rule parameters for the various experiments. VC stands for Visual Cortex cells (for experimental details see [18], * standard set of parameters), SC for Somatosensory Cortex cells (see[32]) and HP for Hippocampal cells (see [12]). Bold numbers indicate the free parameters fitted to experimental data. Other parameters are set in advance to values based on the literature.

Table 1a.

Parameters	Value
C - membrane capacitance	281pF
g_L - leak conductance	30nS
E_L - resting potential	-70.6mV
Δ_T - slope factor	2mV
$V_{T_{rest}}$ - threshold potential at rest	-50.4mV
$\tau_{w_{ad}}$ - adaptation time constant	144ms
a - subthreshold adaptation	4nS
b - spike triggered adaptation	0.805pA
I_{sp} - spike current after a spike	400pA
τ_z - spike current time constant	40ms
τ_{V_T} - threshold potential time constant	50ms
V_{Tmax} - threshold potential after a spike	$30{:}4mV$

1b.

Exper.	$\theta_{-}(mV)$	$\theta_{+}(mV)$	$A_{LTD}\,(mV)^{-1}$	$A_{LTP}\ (mV)^{-2}$	$\tau_x\ (ms)$	$\tau_{-}\ (ms)$	$\tau_{+}\ (ms)$
VC*	-70.6	-45.3	$\mathbf{14}e^{-5}$	$\mathbf{8}e^{-5}$	**15**	**10**	**7**
SC	-70.6	-45.3	$\mathbf{21}e^{-5}$	$\mathbf{30}e^{-5}$	**30**	**6**	**5**
HP	**-41**	**-38**	$\mathbf{38}e^{-5}$	$\mathbf{2}e^{-5}$	16		

5. Methods

6.1 Neuron Model

In contrast to standard models of STDP, the plasticity model presented in this paper involves the postsynaptic membrane potential *u*(t). As a model for neuronal voltage, we chose the Adaptive Exponential Integrate-and-Fire (AdEx) model (Brette and Gerstner, 2005) with an additional current describing the depolarizing spike after potential (Badel et al. 2008). The voltage evolution is

$$C\frac{d}{dt}u = -g_L(u - E_L) + g_L\Delta_T e^{\frac{u-V_T}{\Delta_T}} - w_{ad} + z + I,$$

where *C* is the membrane capacitance, g_L the leak conductance, E_L the resting potential and *I* the stimulating current. The exponential term describes the activation of sodium current. The parameter Δ_T is called the slope factor and V_T the threshold potential. A hyperpolarizing adaptation current is described by the variable w_{ad} with dynamics

$$\tau_{w_{ad}}\frac{d}{dt}w_{ad} = a\,(u - E_L) - w_{ad},$$

where $\tau_{w_{ad}}$ is the time constant of the adaption of the neuron and *a* a parameter. Upon firing the variable *u* is reset to a fixed value V_{reset} whereas w_{ad} is increased by an amount *b*. The main difference to the Izhikevich model [25] is that the voltage is exponential rather than quadratic allowing a better fit to data (Badel et al. 2008). The spike afterpotential of the cells used in typical STDP experiments [18] have a long depolarizing spike after potential. We therefore add an additional current *z* which is set to a value I_{sp} immediately after a spike occurs and decays otherwise with a time constant τ_z

$$\tau_z\frac{d}{dt}z = -z.$$

Finally, refractoriness is modeled with a adaptive threshold V_T which starts at $V_{T_{max}}$ after a spike and decays to $V_{T_{rest}}$ with a time constant τ_{V_T} (Badel et al. 2008), i.e.

$$\tau_{V_T} \frac{d}{dt} V_T = -\left(V_T - V_{T_{rest}}\right).$$

Parameters for the neuron model are taken from Brette and Gerstner 2005 for the AdEx, τ_z is set to 40ms in agreement with [18] (see also Badel et al. 2008) and kept fixed throughout all simulations (see table 1A).

6.2 Plasticity Model

Our model exhibits separate additive contributions to the plasticity rule, one for LTD and another one for LTP [30]. For the LTD part, we assume that presynaptic spike arrival at synapse *i* induces depression of the synaptic weight w_i by an amount $-A_{LTD}\,[\bar{u}_-(t) - \theta_-]_+$ .The brackets $[\ ]_+$ indicate rectification, i.e. any value $\bar{u}_-<\theta_-$ does not lead to a change [11] (see Fig 1h). The quantity $\bar{u}_-(t)$ is an exponential low-pass filtered version of the postsynaptic membrane potential *u(t)* with time constant τ_- :

$$\tau_- \frac{d}{dt} \bar{u}_-(t) = -\bar{u}_-(t) + u(t).$$

The variable $\bar{u}_-$ is an abstract variable which could, for instance, reflect the level of calcium concentration [19] or the release of endocannabinoids [44], though such an interpretation is not necessary for our rule. Since the presynaptic spike train is described as a series of short pulses at time t_i^n where *i* is the index of the synapse and *n* an index that counts the spike, $X_i(t) = \sum_n \delta(t - t_i^n)$, we have for depression

$$\frac{d}{dt} w_i^- = -A_{LTD}(\bar{u})X_i(t)[\bar{u}_- - \theta_-]_+ \quad \text{if} \quad w_i > w_{min}, \tag{1}$$

where $A_{LTD}(\bar{u})$ is an amplitude parameter that is under the control of homeostatic processes[31] . For slice experiments the parameter has a fixed value extracted from experiment. For network simulations in Figs. 5-7, we make it depend on the mean depolarization $\bar{u}_-$ of the postsynaptic neuron, averaged over a time scale of 1 second. Eq. 1 is a simple method to implement homeostasis; other methods such as weight rescaling would also be possible[31]. The time scale of 1 second is not critical (100 seconds or more would be more realistic for homeostasis), but convenient for the numerical implementation.

For the LTP part, we assume that each presynaptic spike at the synapse w_i increases the trace $\bar{x}_i(t)$ of some biophysical quantity, which decays exponentially with a time constant τ_x [14,29]

$$\tau_x \frac{d}{dt} \bar{x}_i(t) = -\bar{x}_i(t) + X_i(t),$$

where $X_i(t)$ is the spike train defined above. The quantity $\bar{x}_i(t)$ could for example represent the amount of glutamate bound to postsynaptic receptors[29] or the number of NMDA receptors in an activated state[28]. Potentiation is given by

$$\frac{d}{dt} w_i^+ = +A_{LTP}\,\bar{x}_i(t)[u - \theta_+]_+\,[\bar{u}_+ - \theta_-]_+ \qquad \text{if} \quad w_i < w_{max}. \tag{2}$$

Here, A_{LTP} is a free amplitude parameter fitted to the data and $\bar{u}_+$(t) is another low-pass filtered version of *u(t)* similar to $\bar{u}_-$(t) but with a shorter time constant τ_+ around 10ms. Thus positive weight changes can occur if the momentary voltage *u(t)* surpasses a threshold θ_+ and, at the same time the average value $\bar{u}_+$(t) is above θ_-.

The final rule used in the simulation is

$$\frac{d}{dt}w_i = -A_{LTD}(\bar{\bar{u}})X_i(t)[\bar{u}_- - \theta_-]_+ + A_{LTP}\bar{x}_i(t)[u - \theta_+]_+ [\bar{u}_+ - \theta_-]_+ , \qquad (3)$$

combined with hard bounds $w_{min} \leq w_i \leq w_{max}$. For network simulation, $A_{LTD}(\bar{\bar{u}}) = A_{LTD}\frac{\bar{\bar{u}}^2}{u_{ref}^2}$ where u_{ref}^2 is a reference value.

It is unlikely that the model can be simplified further. First, voltage is necessary as a variable whenever voltage is manipulated in experiments, and second, dependence upon voltage must be nonlinear [11-12]. Phenomenological models have some freedom, in the choice of the mathematical form of the nonlinearities (e.g., exponential, polynomial Hill-functions, or piecewise linear) and we chose a suitable combination of piecewise linear functions with thresholds θ_+ and θ_-. Third, STDP experiments indicate that the temporal relation between stimulation events is important. All timing relations have been implemented as (first-order) linear filtering. For the case of classical STDP experiments, where all spikes are triggered by the experimenter our phenomenological model can be simplified and becomes identical or closely related to existing nonlinear STDP models [28-29], but regarding the interaction between voltage and spike timing such a further simplification is not possible. Finally, the fact that the curve of burst-timing dependent plasticity (Fig. 3c) is not perfectly reproduced indicates that our plasticity model does not have an unnecessarily large number of free parameters.

6.3. Analysis of Plasticity Model

We establish a quantitative link between the novel plasticity model (Eq. 3) and BCM theory[26] under the assumption of a linear Poisson (LP) neuron model with spikes. In a LP neuron, input spike trains $X_j(t) = \sum_j \delta(t - t_j^f)$ are low-pass filtered and weighted to give a subthreshold potential $u^s(t) = \sum_j \int_0^\infty \varepsilon(s)X_j(t-s)ds$ where $\varepsilon(s)$ is the time course of an EPSP and u^s is measured with respect to the resting potential θ_-. The LP neuron generates spikes stochastically with stochastic firing intensity ν^{post} proportional (with parameter $1/\alpha$) to u^s, hence the probability of firing in a short time between *t* and *t*+Δ is $P_F(t; t+\Delta) = \nu^{post}(t)\Delta = u^s(t)\,\Delta/\alpha$. If the LP neuron spikes at time t_f^{post}, we add a short voltage pulse $\beta\delta(t - t_f^{post})$. The total membrane potential is therefore

$$u(t) = u^s(t) + \beta\, Y(t) + \theta_- , \qquad (4)$$

where $Y(t) = \sum_f \delta\,(t - t_f^{post})$ is the spike train of the postsynaptic neuron and β is the integral weight of spikes. To illustrate the significance of β suppose that in a hypothetical experiment of 100ms duration we find a single triangular action potential with amplitude 120mV and 1ms duration at half-maximum, and otherwise the voltage is constant at a value of 2mV above rest, then the *mean* voltage averaged over this 100ms period is $\int_0^{100} \mathrm{u(t)dt}/100 \;= 2\mathrm{mV} + 1.2\mathrm{mV} + \theta\_$ so that the weight parameter β in Eq. (4) should have a value of 1.2mV.

By construction the expected number of spikes of the LP neuron is equal to its instantaneous rate $< Y > (t) \;=\; \nu^{post}(t) \;=\; u^s(t)/\alpha$. In the following derivation the time dependence of the variables is not explicitly denoted for the sake of simplicity (except for a few special cases), e. g. *u(t)* is abbreviated as *u*.

We assume that the neuron has *N* excitatory synapses stimulated by *N* presynaptic Poisson spike trains of rates $\nu^{pre} = (\nu_1^{pre} \;, \ldots, \nu_{N1}^{pre} \;)$. Further, we assume that the presynaptic rates ν^{pre} are slowly varying quantities compared to the intrinsic time scales τ_+, τ_- of our plasticity model or those our neuron model (e.g. EPSP duration), which are all below 50ms. This assumption explicitly results in the following simplifications: $\bar{\nu}^{pre} \approx \nu^{pre}$, $\bar{\nu}_-{}^{post} \approx \nu^{post}$ and $\bar{\nu}_+{}^{post} \approx \nu^{post}$. (Notation: For a variable *q*, $\bar{q}$ denotes low-pass filtering with time constant τ_q, $\bar{q}_+$ and $\bar{q}_-$ correspond to the time constants τ_+ and τ_- respectively).

Using the LP model defined above in the plasticity rule (Eq. 3) yields (if we suppress for the moment the dependence upon the homeostatic variable $\bar{\bar{u}}$)

$$\frac{d}{dt} w_i \;=\; -A_{LTD} X_i(t)(\bar{u}_-^s + \beta\, \bar{Y}_-) + A_{LTP} \bar{x}_i(t) \;\; \beta Y(\bar{u}_+^s + \beta\, \bar{Y}_+), \qquad (5)$$

where it was used that (i) θ_- is equal to the resting potential; (ii) all voltage are above resting potential since only excitatory inputs are considered; and (ii) only *Y* is above the firing threshold θ_+ since u^s is the subthreshold voltage. Now we take the average $< . >_{post}$ over the postsynaptic spikes given the postsynaptic rate ν^{post}:

$$< \frac{d}{dt} w_i >_{post} \;=\; -(\alpha + \beta) A_{LTD} X_i(t) \bar{\nu}_-{}^{post} + (\alpha + \beta) A_{LTP} \bar{x}_i(t) \;\; \beta \nu^{post} \bar{\nu}_+{}^{post}. \qquad (6)$$

Here we have used $< Y(t) \bar{Y}_+(t) >_{post}$ $= \nu^{post}$ (t) $\bar{\nu}_+{}^{post}$ (t) which holds because $\bar{Y}_+(t)$ is not influenced by a possible spike at time *t* (just by spikes at times *s* with *s<t*) and it is thus uncorrelated with *Y(t)* given ν^{post}. For slowly varying input rates:

$$< \frac{d}{dt} w_i >_{post} \;=\; -(\alpha + \beta) A_{LTD} X_i(t) \nu^{post} + (\alpha + \beta) A_{LTP} \bar{x}_i(t) \;\; \beta \nu^{post} \nu^{post}. \qquad (7)$$

Taking the average $<.>_{pre}$ over the presynaptic spikes given the presynaptic firing rates ν^{pre} neglecting spike-spike correlations (i. e. correlations between X_i and ν^{post} beyond rate correlations between ν^{pre} and ν^{post}) gives:

$$< \frac{d}{dt} w_i >_{post} = -(\alpha + \beta) A_{LTD} \nu_i{}^{pre} \nu^{post} + (\alpha + \beta) A_{LTP} \nu_i{}^{pre} \beta \nu^{post} \nu^{post}$$

$$= (\alpha + \beta) \beta A_{LTP} \nu_i{}^{pre} \nu^{post} \left(\nu^{post} - \frac{A_{LTD}}{\beta A_{LTP}} \right). \quad (8)$$

Here $<<.>_{post}>_{pre}$ was abbreviated as < . >. The factor $(\alpha + \beta)\beta$ can be interpreted as the learning rate in a rate-based plasticity model and $\frac{A_{LTD}}{\beta A_{LTP}} = \vartheta$ as the threshold for the transition of LTD to LTP in the `quadratic' BCM model [26]. Since A_{LTD} depends on the slow time scale of homeostatic processes upon the long-term averaged potential $\bar{\bar{u}}$, the threshold ϑ is a sliding one. Just as in the BCM model [26], our plasticity model responds to persistent periods of high activity with an increase in the threshold ϑ.

6.5. Parameters and Data Fitting

For the plasticity experiments in slices, we take $\bar{\bar{u}} = u_{\mathrm{ref}}$ as fixed and fit the parameters A_{LTD}. The total number of parameters of the plasticity model is then 7. For all data sets, except the one taken from [12], the threshold θ_- is set to the resting potential and θ_+ to the firing threshold of the AdEx model, i.e. θ_- =-70.6mV and θ_+ =-45.3mV. The remaining five parameters τ_x, τ_-, τ_+, A_{LTD} and A_{LTP} are fitted to each data set individually by the following procedure. We calculate the theoretically predicted weight change $\Delta w_i^{th,j}$ by integrating (analytically or numerically) Eq. 3, for a given experimental protocol *j*, as a function of the free parameters. We then estimate the free parameters by minimizing the mean-square error *E* between the theoretical calculations and the experimental data $\Delta w_i^{exp,j}$:

$$E = \sum_j \left(\Delta w_i^{th,j} - \Delta w_i^{exp,j} \right)^2 .$$

For the data set in hippocampus [12], we also fit the two parameters θ_- and θ_+ since completely different preparations and cell type were used. Moreover for this data set, the time constant τ_x is taken from physiological measurements given in [10] and fixed to the values of 16ms. The parameters for the various experiments are summarized in Table 1B.

6.6. Protocols and mathematical methods

Voltage clamp experiment. (Fig. 1h) The postsynaptic membrane potential was switched in the simulations to a constant value u_{clamp} chosen from -80mV to 0mV while synapses were stimulated with either 25 (blue line) or 100 pulses (red line) at 50Hz. Due to voltage clamping, the actual value of the voltage *u* itself and the low-pass filtered versions $\bar{u}$ are constant and equal to u_{clamp}. Hence, the synaptic plasticity rule becomes

$$\frac{d}{dt}w_i = -A_{LTD}X_i(t)\left[u_{clamp} - \theta_-\right]_+ + A_{LTP}\bar{x}_i(t)\left[u_{clamp} - \theta_+\right]_+ \left[u_{clamp} - \theta_-\right]_+ .$$

STDP experiment and Frequency dependence. (Fig. 2b) Presynaptic spikes in the simulation were paired with postsynaptic spikes that were either advanced by +10ms or delayed by -10ms with respect to the presynaptic spike. Postsynaptic spikes were triggered by brief strong current pulses into the postsynaptic neuron. The pairing was repeated 5 times with different frequencies ranging from 0.1 to 50Hz. These 5 pairings were repeated 15 times at 0.1Hz. However, the 5 pairings at 0.1Hz were repeated only 10 times to mimic the experimental protocol [18].

Burst-timing-dependent plasticity. Fig. 3a: The presynaptic spike is paired Δt=+10ms before (or Δt=-10ms after) 1, 2 or 3 postsynaptic spikes. The frequency of the burst is 50Hz. The neuron receives 60 pairings at a frequency of 0.1Hz. Fig. 3b: The presynaptic spike is paired with a burst of 3 action potentials (Δt=+10ms and -10ms), while the burst frequency varies from 20 to 100Hz. Fig. 3c: A presynaptic spike is paired with a burst of 3 postsynaptic action potentials with burst frequency of 50Hz. The time Δt between the presynaptic spike and the first postsynaptic action potential varies from -80 to 40ms. For a detailed description of the experiments see [32].

Poisson input for functional scenarios. (Fig. 4-7) Poisson inputs are used in all the following experiments. They are generated by a stochastic process where the spike is elicited with a stochastic intensity *v*.

Relation between connectivity and coding: Toy model. (Fig. 4) Weights of ten all-to-all connected neurons are initialized at 1, bounded between 0 and 3. Weights evolve with the voltage-based rule (Eq. 3) for 100s. The model is compared to a canonical pair-based STDP model written as $\frac{d}{dt}w_i = -A_{LTD}^{pair}X_i\bar{y} + A_{LTP}^{pair}\bar{x}_iY$, where *Y* is the postsynaptic spike train defined the same way as the presynaptic spike train X_i with a filter of the postsynaptic spikes $\bar{y}$ similar to $\bar{x}_i$. The parameters are chosen $A_{LTD}^{pair} = A_{LTP}^{pair} = 1e^{-5}$ for the amplitudes and τ_x for the time constant of $\bar{x}_i$ as well as for the time constant of the postsynaptic low-pass filter $\bar{y}$. Rate code: Neuron 1 fires at 2Hz, neuron 2 at 4Hz... neuron 10 at 20Hz following Poisson statistics, i.e. short current pulses are injected to make the neuron fire with Poisson statistics at this frequency. Temporal code: Neurons fire successively every 20ms, first neuron 1 fires then 20ms later neuron 2 then... 10 then 1 etc, in a loop.

Rate coding in network simulation. (Fig. 5) Five hundred presynaptic Poisson neurons with firing rates $\nu_i^{pre}\ (1 \le i \le 500)$ are connected to 10 postsynaptic excitatory neurons. The input rates ν_i^{pre} follow a Gaussian profile, i. e. $\nu_i^{pre} = Ae^{\frac{-(i-\mu)^2}{2\sigma^2}}$, with variance σ = 10 and amplitude A=30Hz. The center μ of the Gaussian shifts randomly every 100ms between 10 different positions equally distributed. Circular boundary conditions are assumed, i.e. neuron *i*=500 is considered as neighbor of *i*=1. Synaptic weights of the feedforward connections to the excitatory neurons are initialized randomly (uniformly in [0.5,2]) and hard bound are set to 0 and 3. The 10 excitatory neurons are all to all recurrently connected with a starting synaptic weight of 0.25 (hard bounds set to 0 and 0.75). In addition, 3 inhibitory neurons are driven by 8 excitatory neurons and the feedforward inputs, they project on 6 excitatory neurons,

connectivity chosen randomly. Those random recurrent connections are fixed and have a weight equal to 1. The feedforward connections onto the inhibitory neurons are also fixed and chosen randomly between 0 and 0.5. The reference value is set to $u_{ref}^2 = 60mV^2$ and the simulation time to 1000s. Parameters are normally chosen as in Table 1B, visual cortex data, except for Fig. 5b-e, where A_{LTP} and A_{LTD} were reduced by a factor 100.

Temporal coding in network simulation. (Fig. 6) Same setting as before but patterns are presented for 20ms successively (from center position 50, to 100, to 150 etc in a circular manner). The reference value has been set to $u_{ref}^2 = 80mV^2$. We use an asymmetry index calculated by the following procedure: first we relabel neurons according to the current position of their receptive field so that with the cyclic stimulation they get activated one after the other: $n \rightarrow n+1 \ldots \rightarrow n+k \rightarrow n-1 \rightarrow n$. We then compare the connections from *n* to *n+k* to that from *n* to *n-k* and compute $AS = \sum_k w_{n,n+k} - w_{n,n-k}$, *k* = 1-3.

Connectivity patterns were also analyzed in model networks where neurons receive (in addition to feedforward and lateral input) unspecific stochastic background activity that makes them fire spontaneously (Supplementary Figure S1).

ICA-like computation - Orientation selectivity with natural images. (Fig. 6) Ten natural images have been taken from the benchmark of Olshausen et al. [37]. A small patch of 16 by 16 pixels from any of the images is randomly chosen every 200ms which is on the order of the fixation time between saccades. Half of the time the image matrix is transposed, flipped around the vertical axis or the horizontal axis in order to remove any statistical orientation bias. After prewhitening, the inputs for the "ON" ("OFF") image are Poisson spike trains generated by the positive (negative) part of the patch (with respect to a reference grey value reflecting the ensemble mean) with maximum frequency of 50Hz. The 2x16x16 inputs are connected to one postsynaptic neuron. The initial weights are set randomly between 0 and 2 and hard bounds are set between 0 and 3. The connections follow the synaptic rule (Eq. 3) where the reference value is set to $u_{ref}^2 = 50mV^2$. Parameters are chosen as in Table 1B (visual cortex data) but A_{LTP} and A_{LTD} were reduced by a factor 10. Every 20 s an extra normalization is applied to equalize the norm of the "ON" weights to the one of the "OFF" weights [27].

References in Methods section:

Brette, R. and Gerstner, W. Adaptive exponential integrate-and-fire model as an effective description of neuronal activity. *J. Neurophysiol.*, **94**:3637-3642 (2005).

Badel, L. et al. Dynamic I-V curves are reliable predictors of naturalistic pyramidal-neuron voltage traces. *J Neurophysiol*, **99**:656-666 (2008).

References

1 **Buonomano, D. V. & Merzenich, M. M. Cortical plasticity: From synapses to maps. *Annual Review of Neuroscience* 21, 149-186 (1998).**

2 Fregnac, Y. & Shulz, D. Activity-dependent regulation of receptive field properties of cat area 17 by supervised Hebbian learning. *J. Neurobiol* 41, 69-82 (1999).
3 Song, S., Sjöström, P. J., Reigl, M., Nelson, S. & Chklovskii, D. B. Highly Nonrandom Features of Synaptic Connectivity in Local Cortical Circuits. *PLoS Biology* 3, 507-519 (2005).
4 Lefort, S., Tomm, C., Sarria, J. C. F. & Petersen, C. C. H. The excitatory neuronal network of the C2 barrel column in mouse primary somatosensory cortex. *Neuron* 61, 301-316 (2009).
5 Denk, W. & Horstmann, H. Serial block-face scanning electron microscopy to reconstruct three-dimensional tissue nanostructure. *PLoS Biol* 2(11), e329. doi:310.1371/journal.pbio.0020329 (2004).
6 Yuste, R. & Bonhoeffer, T. Genesis of dendritic spines: insights from ultrastructural and imaging studies. *Nat Rev Neurosci* 5, 24-34 (2004).
7 Hebb, D. O. *The Organization of Behavior*. (Wiley, 1949).
8 Malenka, R. C. & Bear, M. F. LTP and LTD: An Embarassment of Riches. *Neuron* 44, 5-21 (2004).
9 Markram, H., Lübke, J., Frotscher, M. & Sakmann, B. Regulation of synaptic efficacy by coincidence of postsynaptic APs and EPSPs. *Science* 275, 213-215 (1997).
10 Bi, G. Q. & Poo, M. M. Synaptic modifications in cultured hippocampal neurons: dependence on spike timing, synaptic strength, and postsynaptic cell type. *J. Neurosci.* 18, 10464-10472 (1998).
11 Artola, A., Bröcher, S. & Singer, W. Different voltage-dependent thresholds for inducing long-term depression and long-term potentiation in slices of rat visual cortex. *Nature* 347, 69-72 (1990).
12 Ngezahayo, A., Schachner, M. & Artola, A. Synaptic Activity Modulates the Induction of Bidirectional Synaptic Changes in Adult Mouse Hippocampus. *The Journal of Neuroscience* 20(7), 2451-2458 (2000).
13 Dudek, S. M. & Bear, M. F. Bidirectional long-term modification of synaptic effectiveness in the adult and immature hippocampus. *J. Neuroscience* 13, 2910-2918 (1993).
14 Gerstner, W., Kempter, R., Van Hemmen, L. & Wagner, H. A neuronal learning rule for sub-millisecond temporal coding. *Nature* 383, 76-78 (1996).
15 Legenstein, R., Naeger, C. & Maass, W. What can a Neuron learn with Spike-Timing-Dependent Plasticity? *Neural Computation* 17, 2337-2382 (2005).
16 Gerstner, W. & Kistler, W. M. *Spiking neuron models*. (Cambridge University Press New York, 2002).
17 Lisman, J. & Spruston, N. Postsynaptic depolarization requirements for LTP and LTD: a critique of spike timing-dependent plasticity. *Nature Neuroscience* 8, 839-841 (2005).
18 Sjöström, P. J., Turrigiano, G. G. & Nelson, S. B. Rate, Timing and Cooperativity Jointly Deterimine Cortical Synaptic Plasticity. *Neuron* 32, 1149-1164 (2001).
19 Shouval, H. Z., Bear, M. F. & Cooper, L. N. A unified model of NMDA receptor dependent bidirectional synaptic plasticity. *Proc. Natl. Acad. Sci. USA* 99, 10831-10836 (2002).
20 Lisman, J. E. & Zhabotinsky, A. M. A model of synaptic memory: A CaMKII/PP1 switch that potentiates transmission by organizing an AMPA receptor anchoring assembly. *Neuron* 31, 191-201 (2001).
21 Song, S. & Abbott, L. F. Cortical Development and Remapping through Spike Timing-Dependent Plasticity. *Neuron* 32, 339-350 (2001).
22 Lubenov, E. V. & Siapas, A. G. Decoupling through Synchrony in Neuronal Circuits with Propagation Delays. *Neuron* 58, 118-131 (2008).
23 Levy, N., Horn, D., Meilijson, I. & Ruppin, E. Distributed synchrony in a cell assembly of spiking neurons. *Neural Networks* 14, 815-824 (2001).

24 **Morrison, A., Aertsen, A. & Diesmann, M. Spike-timing dependent plasticity in balanced random networks. *Neural Computation* 19, 1437-1467 (2007).**

25 **Izhikevich, E. M. & Edelman, G. M. Large-scale model of mammalian thalamocortical systems. *Proceedings of the National Academy of Sciences* 105, 3593-3598 (2008).**

26 **Cooper, L. N., Intrator, N., Blais, B. S. & Shouval, H. Z. *Theory of cortical plasticity.*, (World Scientific, 2004).**

27 **Miller, K. D. A model for the development of simple cell receptive fields and the ordered arrangement of orientation columns through activity dependent competition between ON- and OFF-center inputs. *J. Neurosci.* 14, 409-441 (1994).**

28 **Senn, W., Tsodyks, M. & Markram, H. An algorithm for modifying neurotransmitter release probability based on pre- and postsynaptic spike timing. *Neural Computation* 13, 35-67 (2001).**

29 **Pfister, J.-P. & Gerstner, W. Triplets of Spikes in a Model of Spike Timing-Dependent Plasticity. *J. Neuroscience* 26, 9673-9682 (2006).**

30 **O'Connor, D. H., Wittenberg, G. M. & Wang, S. S. H. Dissection of Bidirectional Synaptic Plasticity Into Saturable Unidirectional Processes. *Journal of Neurophysiology* 94, 1565-1573 (2005).**

31 **Turrigiano, G. G. & Nelson, S. B. Homeostatic plasticity in the developing nervous system. *Nature Reviews Neuroscience* 5, 97-107 (2004).**

32 **Nevian, T. & Sakmann, B. Spine Ca2+ Signaling in Spike-Timing-Dependent Plasticity. *J. Neurosci.* 26, 11001-11013 (2006).**

33 **Kampa B.M., Letzkus J.J. & Stuart G.J. Requirement of dendritic calcium spikes for induction of spike-timing-dependent synaptic plasticity. J. Physiology 574, 283–290 (2006).**

34 **Kozloski, J. & Cecchi, G. A. Topological Effects of Spike Timing-Dependent Plasticity. *arxiv.org* abs, 0810.0029 (2008).**

35 **Jadhav, S. P., Wolfe, J. & Feldman, D. E. Sparse temporal coding of elementary tactile features during active whisker sensation. *Nature Neuroscience*, doi:10.1038/nn.2328 (2009).**

36 **Blais, B., Shouval, H. & Cooper, L. Receptive field formation in natural scene environments: comparison of single-cell learning rules. *Neural Computation* 10, 1797-1813 (1998).**

37 **Olshausen, B. A. & Field, D. J. Emergence of simple-cell receptive field properties by learning a sparse code for natural images. *Nature* 381, 607-609 (1996).**

38 **Oja, E. A simplified Neuron as a Principal Component Analyzer. *Journal of Mathematical Biology* 15, 267-273 (1982).**

39 **Hyvärinen, A., Karhunen, J. & Oja, E. *Independent Component Analysis*. (Wiley, New York, 2001).**

40 **Wang, H. X., Gerkin, R. C., Nauen, D. W. & Bi, G.-Q. Coactivation and timing-dependent integration of synaptic potentiation and depression. *Nat. Neurosci.* 8, 187-193 (2005).**

41 **Saudargiene, A., Porr, B. & Wörgötter, F. How the shape of pre- and postsynaptic signals can influence STDP: A biophysical model. *Neural Computation* 16, 595-626 (2003).**

42 **Brader, J. M., Senn, W. & Fusi, S. Learning real-world stimuli in a neural network with spike-driven synaptic dynamics. *Neural Computation* 19, 2881-2912 (2007).**

43 **Clopath, C., Ziegler, L., Vasilaki, E., Büsing, L. & Gerstner, W. Tag-Trigger-Consolidation: A Model of Early and Late Long-Term-Potentiation and Depression. *PLoS Comput Biol* 4 (2008)** e1000248. doi:10.1371/journal.pcbi.1000248

44 **Sjöström, P. J., Turrigiano, G. G. & Nelson, S. B. Neocortical LTD via coincident activation of presynaptic NMDA and cannabinoid receptors. *Neuron* 39, 641-654 (2003).**

45 **Sjöström, P. J. & Häusser, M. A Cooperative Switch Determines the Sign of Synaptic Plasticity in Distal Dendrites of Neocortical Pyramidal Neurons. *Neuron* 51, 227-238 (2006).**

46 **Tsodyks, M. & Markram, H. The neural code between neocortical pyramidal neurons depends on neurotransmitter release probability. *Proc. Natl. Academy of Sci., USA* 94, 719-723 (1997).**

47 **Frey, U. & Morris, R. G. M. Synaptic tagging and long-term potentiation. *Nature* 385, 533-536 (1997).**

48 **Remy, S. & Spruston N. Dendritic spikes induce single-burst long-term potentiation. *PNAS* 104-43; 17193-17197 (2007).**

49 **Hardie, J. & Spruston, N. Synaptic Depolarization Is More Effective than Back-Propagating Action Potentials during Induction of Associative Long-Term Potentiation in Hippocampal Pyramidal Neurons. *J. Neurosci* 2009, 29: 3233 - 3241 (2009).**

50 **Golding, N. L., Staff, N. P. & Spruston, N. Dendritic spikes as a mechanism for cooperative long-term potentiation. *Nature* 418, 326-331 (2002).**

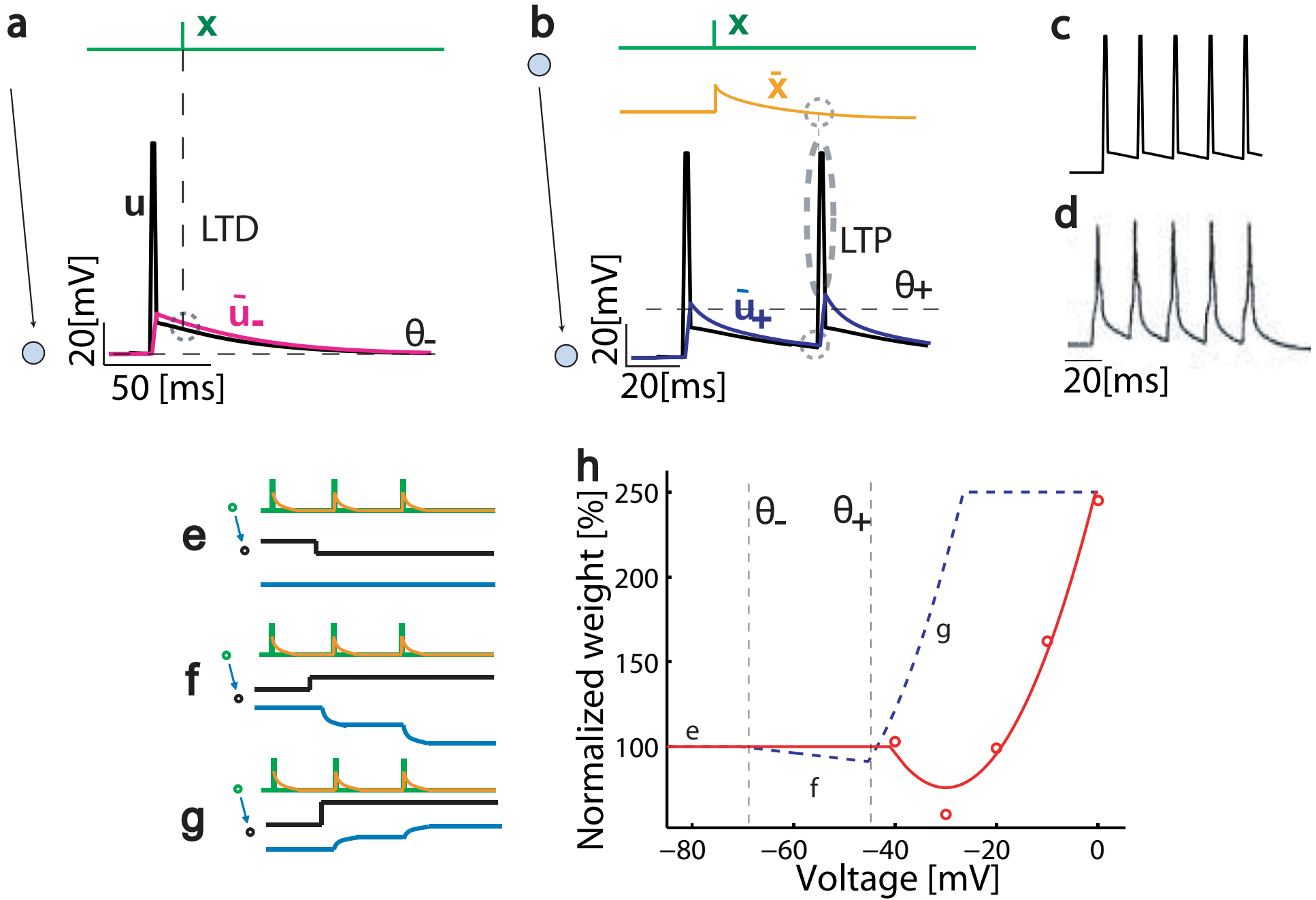
a
x
u
LTD
ū-
θ-
20[mV]
50 [ms]
b
x
x̄
LTP
θ+
ū+
20[mV]
20[ms]
c
d
20[ms]
e
f
g
h
Normalized weight [%]
250
200
150
100
θ-
θ+
e
f
g
−80
−60
−40
−20
0
Voltage [mV]

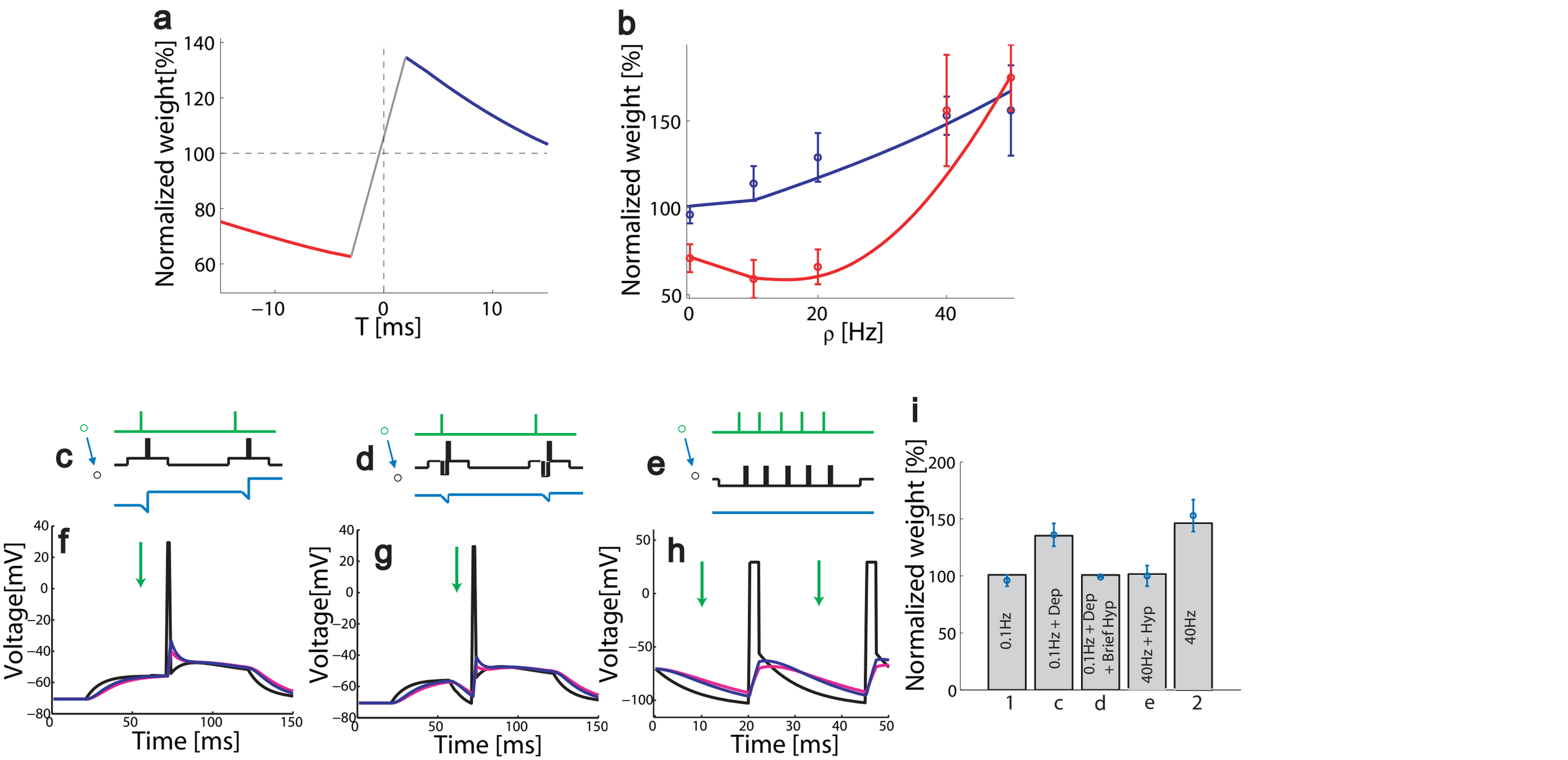
a
Normalized weight[%]
140
120
100
80
60
−10
0
10
T [ms]
b
Normalized weight [%]
150
100
50
0
20
40
ρ [Hz]
c
d
e
f
Voltage[mV]
40
20
0
−20
−40
−60
−80
0
50
100
150
Time [ms]
g
Voltage[mV]
Time [ms]
h
Voltage[mV]
50
0
−50
−100
0
10
20
30
40
50
Time [ms]
i
Normalized weight [%]
200
150
100
50
0
0.1Hz
0.1Hz + Dep
0.1Hz + Dep + Brief Hyp
40Hz + Hyp
40Hz
1
c
d
e
2

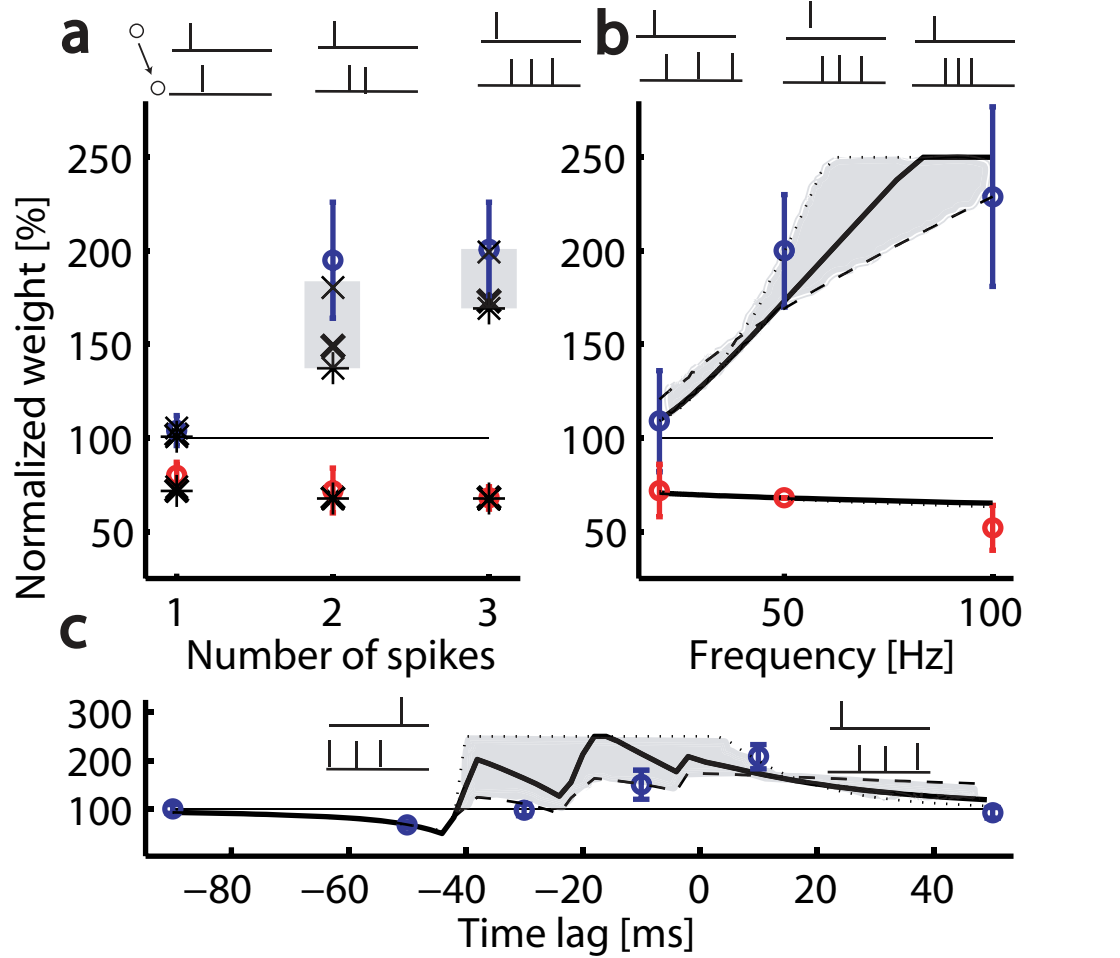
a
b
c
Normalized weight [%]
250
200
150
100
50
1
2
3
Number of spikes
50
100
Frequency [Hz]
300
200
100
−80
−60
−40
−20
0
20
40
Time lag [ms]

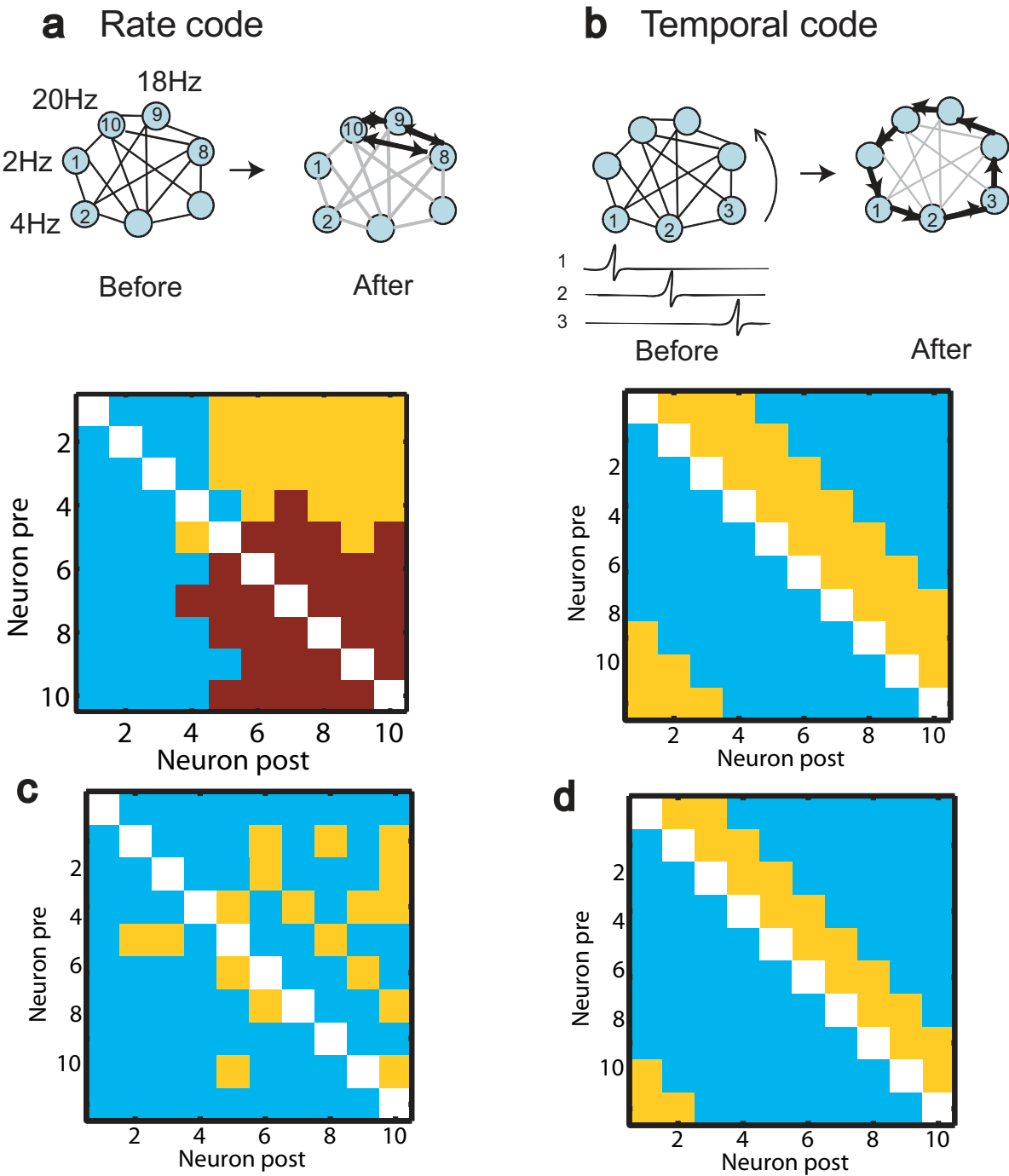
a
Rate code
20Hz
18Hz
2Hz
4Hz
Before
After
b
Temporal code
1
2
3
Before
After
Neuron pre
Neuron post
c
d

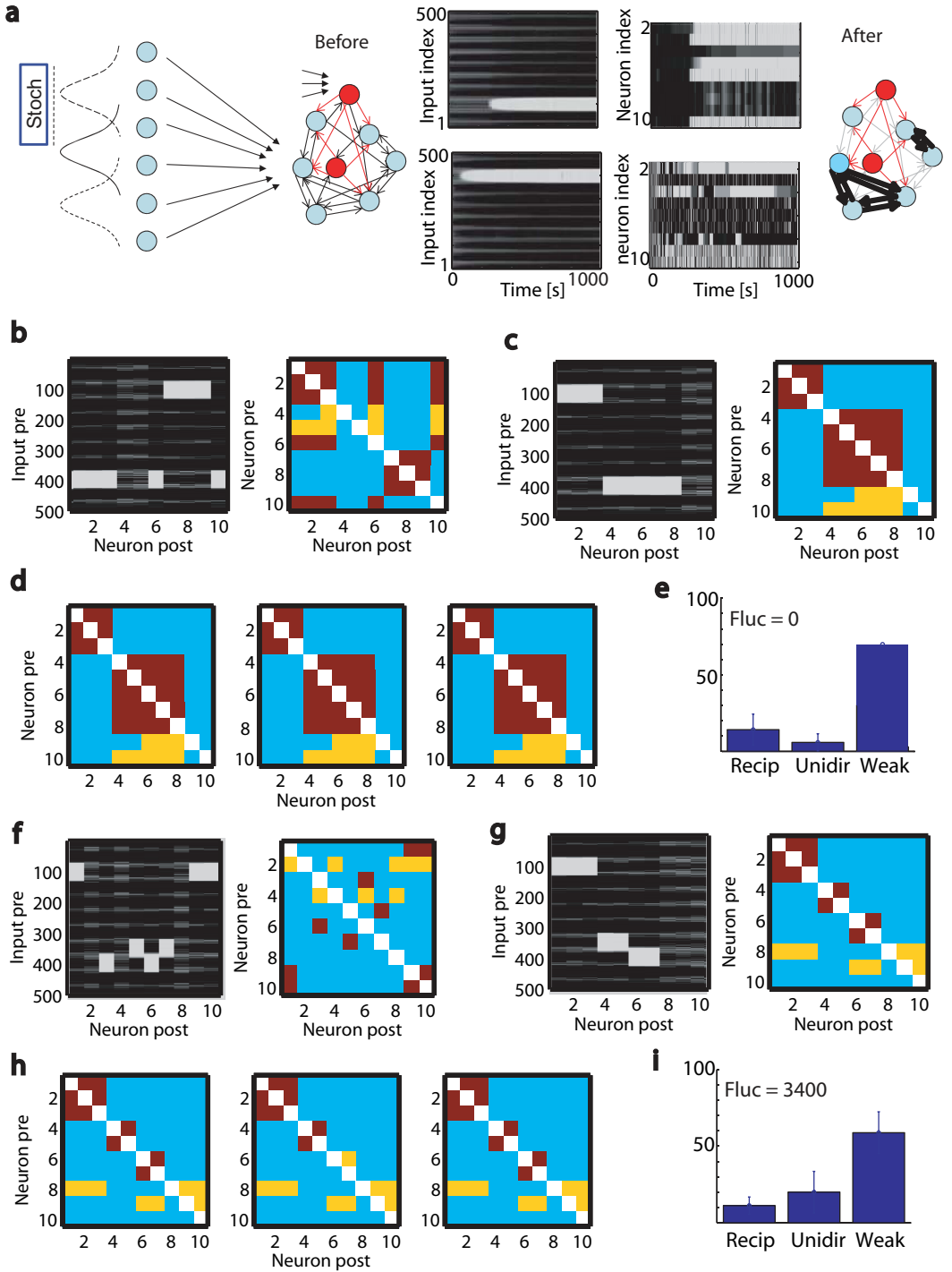
a
Stoch
Before
After
Input index
Neuron index
neuron index
Time [s]
b
c
d
e
Fluc = 0
Recip
Unidir
Weak
f
g
h
i
Fluc = 3400
Input pre
Neuron pre
Neuron post

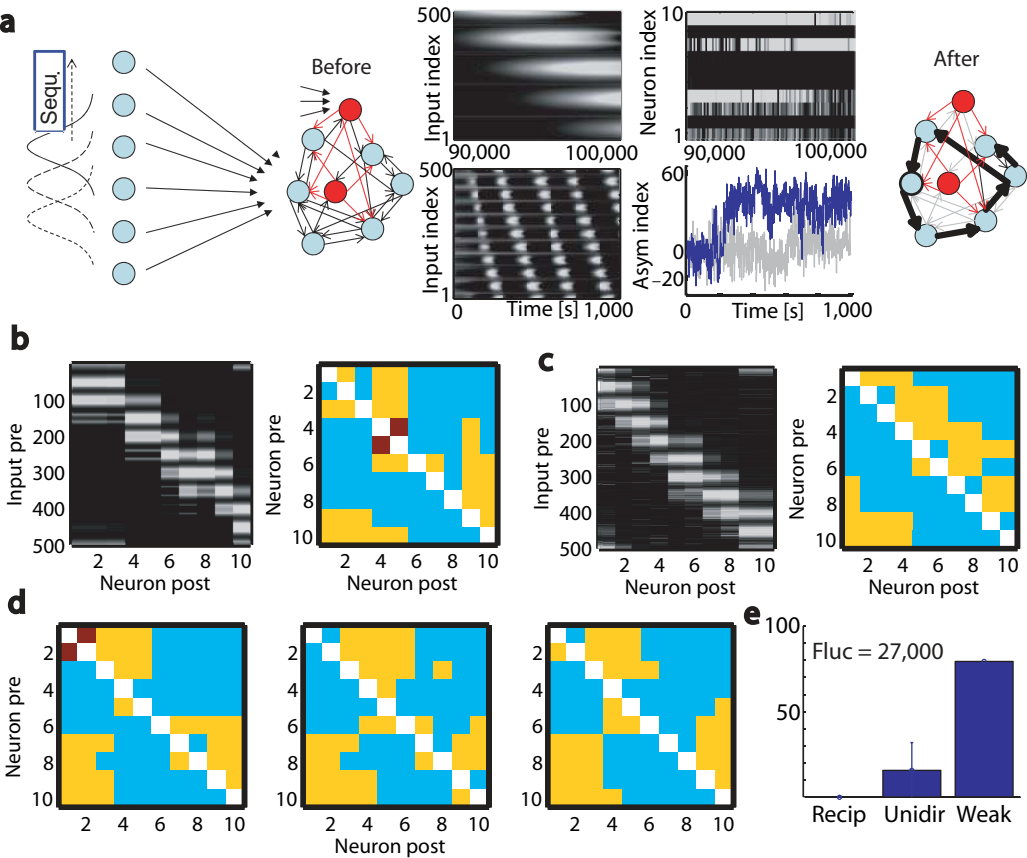
a
Sequ.
Before
After
Input index
Neuron index
Asym index
Time [s]
90,000
100,000
1,000
b
c
d
e
Input pre
Neuron pre
Neuron post
Fluc = 27,000
Recip
Unidir
Weak

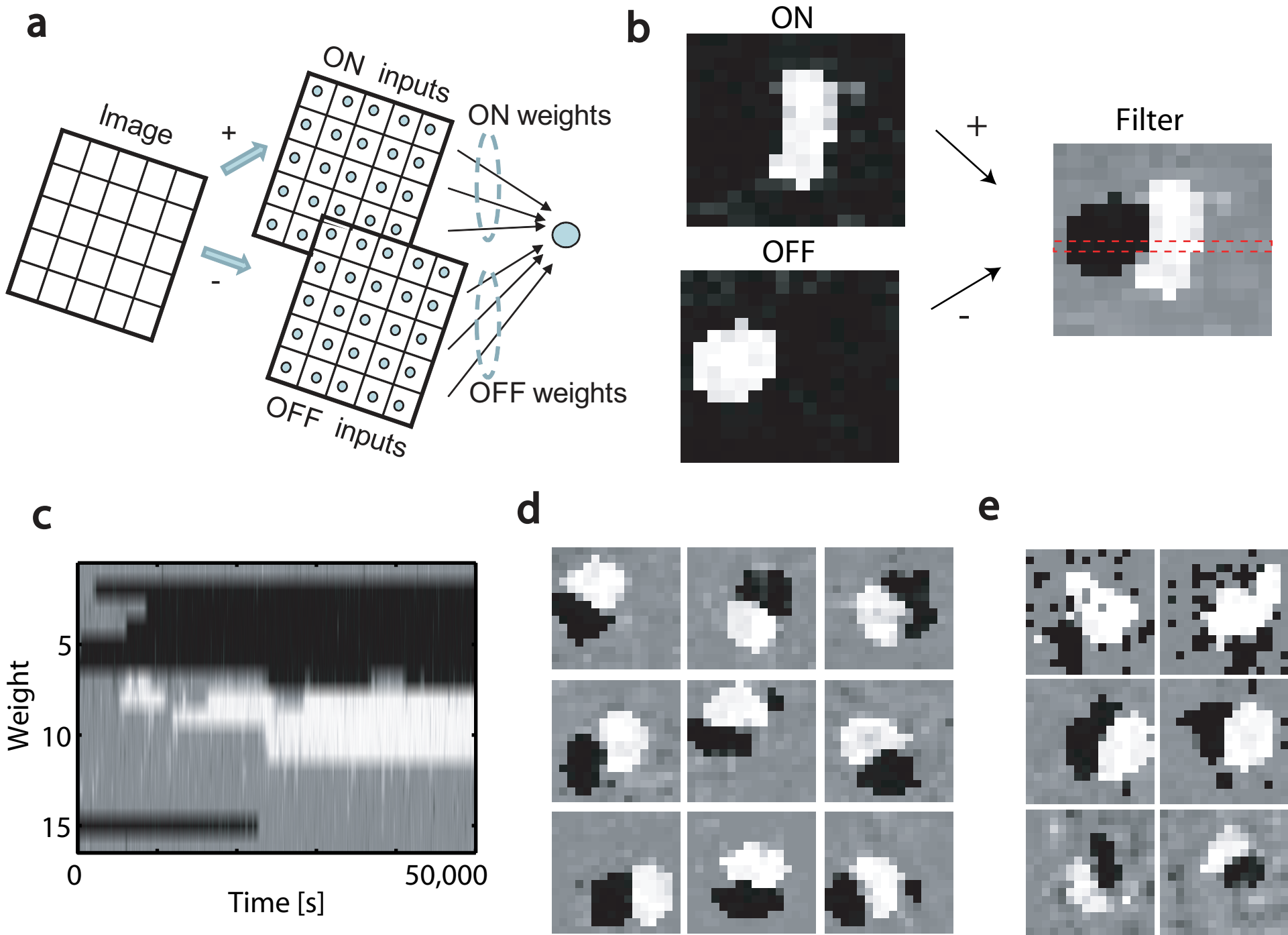
a
Image
+
-
ON inputs
OFF inputs
ON weights
OFF weights
b
ON
OFF
+
-
Filter
c
Weight
5
10
15
0
50,000
Time [s]
d
e

Supplementary Material
Connectivity reflects Coding: A Model of Voltage-based Spike-Timing-Dependent-Plasticity with Homeostasis

Claudia Clopath, Lars Büsing, Eleni Vasilaki, Wulfram Gerstner

1 Calculations for the functional implications

We apply the results derived in methods to the toy model of Fig. 4 and compare results of our rule to those of standard pair-based STDP. We assume that lateral connections are weak, so that neuronal firing is triggered by the injected current pulses. Since we focus on recurrent networks, the weights carry two indices (e. g. w_{ij} for a weight from neuron j to i) and the output spike train of neuron i is denoted as X_i.

1.1 Rate coding

Since in Fig. 4A, current pulses are injected with Poisson distributed timing at fixed rate, neurons i and j exhibit Poisson firing with rates ν_i and $\nu_j > 0$, respectively. From Eq. (8) it follows that all postsynaptic neurons with rate $\nu_i > \vartheta$ have increasing synaptic weights, while all those with $\nu_i < \vartheta$ have decreasing connections. After some time, connections reach their upper or lower bound so that all neurons with $\nu_i > \vartheta$ have input connections with all weights $w_{ij} = w_{\max}$, independent of j and all other neurons have no incoming connections, in agreement with the results of Fig. 4A. Note that in this simulation the threshold ϑ was fixed since the homeostatic control of $A_{\rm LTD}$ was turned off.

Standard STDP. Changes of bidirectional connections induced by STDP in the rate coding scenario (where pre- and postsynaptic activities are independent) are of opposite direction, i. e. if weight w_{ij} is potentiated w_{ji} is depressed. If the the STDP function is antisymmetric with respect to time reversal, i.e. if the amplitude of potentiation at pre-post timing with time different $|\Delta|$ is the same as that of depression with reversed timing, then

$$\Delta w_{ij} = \int\limits_{\text{experiment}} \left(\frac{d}{dt} w_{ij}\right) dt = -\Delta w_{ji}.$$

Hence, STDP cannot produce strong bidirectional weights if weights are initialized with medium strength. Note that bidirectional connections would be possible if the amount of potentiation outweighs the amount of depression, that is, if the integral over the STDP window is positive.

1.2 Temporal Coding

We assume that N neurons are arranged on a circle and fire one of the other $n, n+1, ...$ with an interval of τ. We calculate the weight change Δw_{ij} per firing cycle given that the system has undergone infinitely many firing cycles before. It is also assumed that the voltage trace consists only of the spike events, however, similar results can be obtained if the subthreshold current injection (that makes the neurons spike in the scenario of Fig. 4B) is taken into account.

Because of the cyclic activation pattern, we can evaluate the term $\overline{u}_{i-}$ at a presynaptic spike time of X_j:

$$\int\limits_{\text{cycle}} \overline{u}_{i-} X_j \, dt \quad = \quad \beta \sum_{n=0}^{\infty} \exp\left(-\frac{(j-i) \bmod N \cdot \tau + nN\tau}{\tau_-}\right) \tag{1}$$

Hence the amount of depression per cycle is, after summation,

$$\text{Depression} \quad = \quad \beta A_{\rm LTD} \cdot \exp\left(-\frac{(j-i) \bmod N \cdot \tau}{\tau_-}\right) \frac{1}{1-\exp\left(-\frac{N\tau}{\tau_-}\right)}. \tag{2}$$

For potentiation we have to evaluate $\overline{u}_{i+}\overline{x}_j$ at the time of a postsynaptic spike X_i. Under the above assumptions, the factors $\overline{u}_{i+}$ and $\overline{x}_j$ can be summed up separately, so that the amount of potentiation per cycle is:

$$\text{Potentiation} \quad = \quad A_{\text{LTP}}\beta^2 \frac{1}{\exp\left(\frac{N\tau}{\tau_+}\right) - 1} \cdot \exp\left(-\frac{(i-j) \bmod N \cdot \tau}{\tau_x}\right) \frac{1}{1 - \exp\left(-\frac{N\tau}{\tau_x}\right)}.$$

We note that the depression term scales like $\exp(-(j-i) \bmod N)$, which is largest if the postsynaptic neuron i is directly before presynaptic neuron j in the cycle. For the potentiation term it is just the other way round since it scales like $\exp(-(i-j) \bmod N)$: It takes the largest value if the postsynaptic neuron i is directly after the presynaptic neuron j. Hence weights from n to $n+k$ (for small $k > 0$), i.e, those that are "in cycle direction" are potentiated, and weights "against cycle direction" are depressed. This results in a highly asymmetric connection pattern.

Standard STDP. The calculations are exactly as in the temporal coding case of the novel plasticity rule, except for the factor $\overline{u}_{i+}$ (which does not dependent on i or j and hence is just a global scaling). In this setup the novel rule and STDP behave equivalently.

2 Supplementary Figures

Supplementary Figure 1S - Simulation of the network with background activity

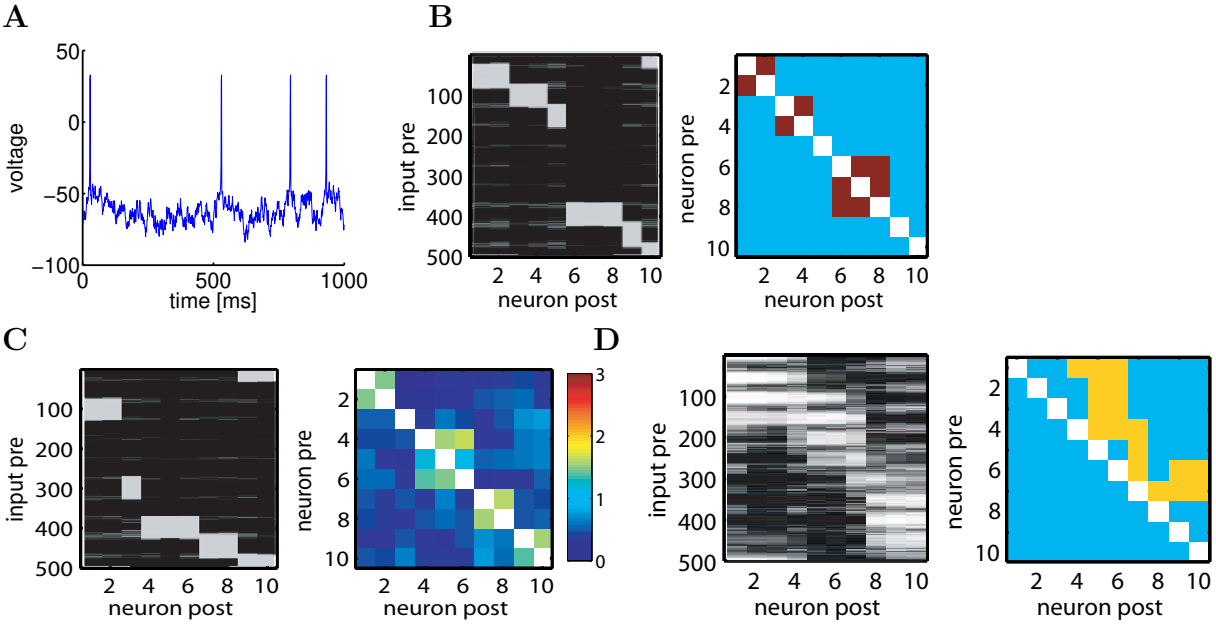

Figure 1S: Network with background activity. A. Each neuron in the network receives a random input current that leads to stochastic firing at 4Hz and large fluctuations of the subthreshold membrane potential. B. The simulation paradigm as in Fig 5C, but in the presence of background activity, leads to strong bidirectional connections (small learning rate). C. The simulation paradigm as in Fig 5G leads to clusters of bidirectional connections D. The simulation paradigm as in Fig 6C leads to unilateral connections

Supplementary Figure 2S - Rate code vs Temporal code: Duration and cycle length of presentation

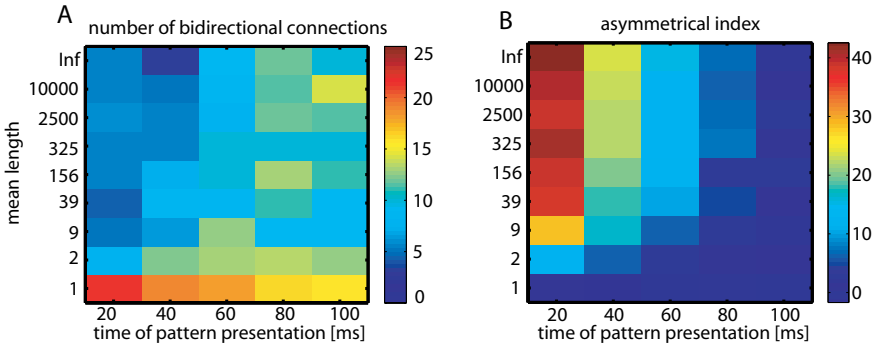

Figure 2S: Stimuli as in Fig 5 and 6 of the main text, except that the duration of stimulus presentation was systematically varied between 20 and 100 ms (horizontal axis) and the cycle length until random restart was varied from 1 to infinity. Figure 5 in the main text corresponds to cycle length 1 (random position of the stimulus) and stimulus duration 100ms, i.e., the lower-right corner. Figure 6 in the main text corresponds to cycle length infinity and stimulus duration 20ms (upper-left corner). To simulate intermediate values of cycle length, we have drawn a random number between zero and one after each presentation of a stimulus. If the random number was above a value p the cycle was continued, else restarted at random position. Changing p gives different expected cycle lengths. The reference value was set to $u^2_{ref} = 70\text{mV}^2$ A. Number of bidirectional connections in the recurrent network. B. Asymmetrical index in the recurrent network.

Supplementary Figure 3S - Dependence upon input rates

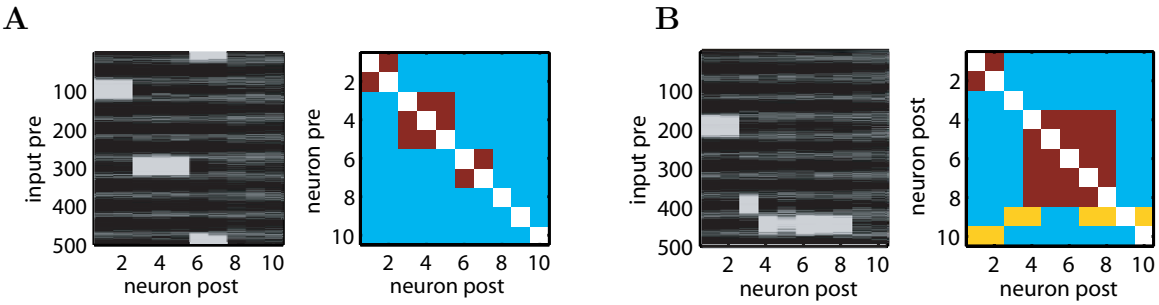

Figure 3S: Intensity of presynaptic stimulation is not important. Stimuli as in Fig 5C and 5G, except that the firing rate of presynaptic inputs was reduced by a factor of 2. A. Learning rate and network as in Fig 5C. B. Learning rate and network as in Fig 5G.

3 Code

```
% parameters of the rule
% A_m:      amplitude for the depression
% A_p:      amplitude for the potentiation
% tau_p:    time constant for voltage trace in the potentiation term [ms]
% tau_x:    time constant for presynaptic trace [ms]
% tau_m:    time constant for voltage trace in the depression term [ms]
% tetam:    low threshold
% tetap:    high threshold in the potentiation term
% x:        presynaptic spike train (here in the case of one presynaptic stimulated cell)
% Is:       train of postsynaptic current injected in the cell
% Iext:     additional current injected in the cell
% T:        length of the simulation


% parameters of the neuron model from Brette et al. 2005
E_L = -70.6;                % resting potential [mV]
C   = 281;                  % membrane capacitance [pF]
V_T = -50.4;                % adaptive threshold
```

```
% initialization
z       = zeros(1,T);        % current for spike after potential
I_sub   = zeros(1,T);        % current due to weighted sum of the presynaptic spikes
I_tot   = zeros(1,T);        % total current
wad     = zeros(1,T);        % adaptation variable
u       = E_L*ones(1,T);     % membrane potential
u_md    = E_L*ones(1,T);     % membrane potential for the depression
u_mp    = E_L*ones(1,T);     % membrane potential for the potentiation
x_m     = zeros(1,T);        % presynaptic trace
w       = 0.5;               % initialization of the weight
counter = 0;                 % ensure spike length of 2ms

% Main loop
for t = 4:T % time
    % current due to presynaptic spike arrival
    I_sub(t) = w*x(t)*C;
    % total current received by the cell
    I_tot(t) = I_sub(t)+ I_s(t)+I_ext(t);
    % neuron model computing the next voltage u
    [u(t), wad(t), z(t), counter, V_T] = ...
          adex(u(t-1), wad(t-1), z(t-1),I_tot(t), counter, V_T);
    % trace of membrane potential (u) with time constant tau_d
    u_md(t+1) = u(t)/tau_d +(1-(1/tau_d))*u_md(t);
    % trace of membrane potential (u) with time constant tau_p
    u_mp(t+1) = u(t)/tau_p +(1-(1/tau_p))*u_mp(t);
    % trace of presynaptic spike train (x)
    x_m(t+1) = x(t)/tau_x +(1-(1/tau_x))*x_m(t);
    % membrane potential (u) thresholded by thetap
    u_sig = (u(t) > tetap)*(u(t)-tetap);
    % membrane potential trace (u_md) thresholded by thetm
    % (taken 3ms before since time of a spike is 2ms)
    u_md_sig = ((u_md(t-3)-tetam) > 0)*(u_md(t-3)-tetam);
    % membrane potential trace (u_md) thresholded by thetm
    u_mp_sig = ((u_mp(t-3)-tetam) > 0)*(u_mp(t-3)-tetam);
    % weight update
    w =  w- A_m*x(t)*u_md_sig+ A_p*u_sig*x_m(t)*u_mp_sig;
end
```